

Polarization study of the P-wave charmonium radiative decay into a light vector meson at e^+e^- collider experiment*

Yong-Qing Chen (陈永清)¹ Peng-Cheng Hong (洪鹏程)^{2†} Zhuo Chen (陈琢)¹
Wei Shan (单蔚)^{1‡} Wei-Min Song (宋维民)^{2§}

¹School of Physics and Electronics, Hunan Normal University, Changsha, China

²College of Physics, Jilin University, Changchun, China

Abstract: In this work, a formalism is presented for the helicity amplitude analysis of the decays $\psi(2S) \rightarrow \gamma_1 \chi_{cJ}, \chi_{cJ} \rightarrow \gamma_2 V (V = \rho^0, \phi, \omega)$ (the subscript 1,2 is used to distinguish the two radiative photons), and the polarization expressions of the P-wave charmonia χ_{cJ} and the vector mesons ρ^0, ϕ, ω for experimental measurements at Electron-Positron Collider. In addition, we derive the formulae of the angular distributions of the $\chi_{c1,2} \rightarrow \gamma V$ to extract the degree of transverse polarization P_T of e^+e^- pairs with symmetric beam energy as well as the ratios of two helicity amplitudes x (in χ_{c1} decays) and x, y (in χ_{c2} decays) representing the relative magnitudes of transverse to longitudinal polarization amplitude, and validate it by performing the Monte Carlo simulation. Finally, the statistical sensitivity of P_T, x and y are estimated based on the large $\psi(2S)$ data samples collected at the current and proposed future e^+e^- collider experiment.

Keywords: P-wave charmonia, polarization, vector meson, angular distribution, spin density matrix

DOI:

I. INTRODUCTION

Over past five decades, heavy quarkonium spectra have been established due to a collective of theorists and experimentalists working. More than 40 heavy quark-antiquark bound states, also known as charmonium and bottomonium, are observed with masses ranging from 2.9 GeV to 4.7 GeV or from 9.3 GeV to 11.1 GeV, respectively [1]. The heavy quarkonia below the open-flavor production mass-threshold are relatively well understood, which provide an ideal laboratory to test perturbative and nonperturbative quantum chromodynamics (QCD) [2, 3].

Charmonium decay is usually a focused research topic that is significant and useful for understanding the fundamental characteristics of charmonium. J/ψ and $\psi(2S)$ are two of the observed charmonium states that have a wealth of experimental decay information, which are recently listed in the Particle Data Group (PDG) [1]. Compared to J/ψ and $\psi(2S)$, the experimental measurement pertinent to the decay of spin singlets, such as the P-wave state h_c and the S-wave state η_c , as well as spin triplets,

the P-wave state χ_{cJ} are significantly less. Therefore, there are currently more active theoretical and experimental investigations into those charmonia decays.

Experimental measurements of charmonium radiative decay to light-quark vector mesons would help us understand the QCD and QED mechanism between charmonium and light vector mesons by strong interaction and electromagnetic interaction. The previous theoretical study for radiative decays of charmonium into light vector mesons, the processes $\chi_{cJ} \rightarrow \gamma V$, is based on numerical calculations for the quark-gluon loop diagrams in perturbative QCD (pQCD) frame and nonrelativistic quantum chromodynamics (NRQCD) [4, 5]. It provides a useful place to investigate the interactions between quarks and gluons in OZI suppressed processes. And its predicted branching ratios of the decays $\chi_{cJ} \rightarrow \gamma V$ have been tested by later e^+e^- collider experiments.

The measurement for the branching ratios of the P-wave charmonia $\chi_{cJ} \rightarrow \gamma V$ have been presented by CLEO-c and BESIII collaborations in 2008 [6] and 2011 [7], respectively. However, there are still some signific-

Received 25 June 2024; Accepted 24 October 2024

* Supported by the National Natural Science Foundation of China (11805064, 11975118)

† E-mail: hongpc@ihep.ac.cn

‡ E-mail: shanw@hunnu.edu.cn

§ E-mail: weiminsong@jlu.edu.cn



Content from this work may be used under the terms of the Creative Commons Attribution 3.0 licence. Any further distribution of this work must maintain attribution to the author(s) and the title of the work, journal citation and DOI. Article funded by SCOAP³ and published under licence by Chinese Physical Society and the Institute of High Energy Physics of the Chinese Academy of Sciences and the Institute of Modern Physics of the Chinese Academy of Sciences and IOP Publishing Ltd

ant discrepancy between the experimental results and the theoretical predictions as shown in **Table 1**. To resolve the discrepancy, an attempt was made to employ a phenomenological model with hadronic loop mechanism [8].

Table 1. Comparison of experimental measurement results (CLEO-c, BESIII) and theoretical calculated results (pQCD, NRQCD, NRQCD+QED) for the branching ratio of $\chi_{cJ} \rightarrow \gamma V (V = \rho^0, \phi, \omega)$ [in unit of 10^{-6}]

Decay Mode	CLEO-c[6]	BESIII [7]	pQCD [4]	NRQCD [5]	NRQCD+QED [5]
$\chi_{c0} \rightarrow \gamma \rho^0$	<9.6	<10.5	1.2	3.2	2.0
$\chi_{c1} \rightarrow \gamma \rho^0$	$243 \pm 19 \pm 22$	$228 \pm 13 \pm 22$	14	41	42
$\chi_{c2} \rightarrow \gamma \rho^0$	<50	<20.8	4.4	13	38
$\chi_{c0} \rightarrow \gamma \phi$	<6.4	<16.2	0.46	1.3	0.03
$\chi_{c1} \rightarrow \gamma \phi$	<26	$25.8 \pm 5.2 \pm 2.3$	3.6	11	11
$\chi_{c2} \rightarrow \gamma \phi$	<13	<8.1	1.1	3.3	6.5
$\chi_{c0} \rightarrow \gamma \omega$	<8.8	<12.9	0.13	0.35	0.22
$\chi_{c1} \rightarrow \gamma \omega$	$83 \pm 15 \pm 12$	$69.7 \pm 7.2 \pm 6.6$	1.6	4.6	4.7
$\chi_{c2} \rightarrow \gamma \omega$	<7.0	<6.1	0.5	1.5	4.2

The Sokolov-Ternov effect induces self-polarization in high-energy e^+e^- beams, which allows them to naturally become transversely polarized in a storage ring [9]. Based on the $(2712 \pm 14) \times 10^6 \psi(2S)$ data samples collected by the BESIII detector in 2009, 2012 and 2021, the precise measurement of polarized parameters and the impact of transversely polarized beams on them will become feasible, enabling a thorough examination of these theoretical models and aiding in a better understanding of the properties of P-wave charmonium radiation decays [10]. Despite the measurement of the branching ratio of $\chi_{cJ} \rightarrow \gamma V$, accurate measurement on their polarized parameters is sensitive to validate theoretical calculation.

In this work, we present a helicity amplitude formula for the process $e^+e^- \rightarrow \psi(2S) \rightarrow \gamma_1 \chi_{cJ} \rightarrow \gamma_1 \gamma_2 V (V = \rho^0, \phi, \omega)$ and construct the spin density matrix for χ_{cJ} and the light vector mesons. The expressions of joint angular distributions are obtained, and some polarization observables are given to be measured in the e^+e^- collider. The statistical sensitivities for the relative magnitudes of transverse to longitudinal polarization amplitude of light vector mesons are also discussed with Monte Carlo (MC) simu-

lation results in the paper. By considering the transverse polarization of e^+e^- pairs, the angular distribution parameters will be measured with a high accuracy as well as other decay parameters.

II. HELICITY AMPLITUDE ANALYSIS

The helicity mechanism is a way to effectively build the dynamic information of the entire decays [11, 12]. The decay planes as well as helicity angles are visually and clearly depicted in **Fig. 1**. In $\psi(2S) \rightarrow \gamma_1 \chi_{cJ}$ decay, the helicity angle θ_1 is the polar angle between the direction of the momenta of e^+ and γ_1 in e^+e^- center-of-mass (CM) frame. In $\chi_{cJ} \rightarrow \gamma_2 V$ decay, the helicity angle θ_2 is chosen as the angle between the direction of momentum of γ_2 in γ_1 rest frame and the direction of momentum of γ_1 from e^+e^- collision, ϕ_2 is the azimuthal angle between the χ_{cJ} production plane and its decay plane. In $\rho^0 \rightarrow \pi^+\pi^-$ and $\phi \rightarrow K^+K^-$ decays, there are two helicity angles, the polar angle θ_3 and the azimuthal angle ϕ_3 , while in a three-body decay $\omega \rightarrow \pi^+\pi^-\pi^0$, we use the Euler angles (α, β, γ) to describe its coordinate system rotating process. Specifically, the γ_1 rest frame is rotated to γ_2 rest frame by γ around z_3 , β around y_3 and finally α around z_3 , where β is the angle between the momentum direction of γ_2 and the cross product direction of the momenta of π^+ and π^- in ω rest frame [13].

These helicity angles can be constructed by the momentum of final particles. One important point to note is the need to transform the experimentally obtained laboratory-frame momentum to the rest frame of the decaying parent particle for calculation.

The helicity angles and amplitudes for sequential decays are defined in **Table 2**. The total amplitude \mathcal{M} for the sequential decay $\psi(2S) \rightarrow \gamma_1 \chi_{cJ} \rightarrow \gamma_1 \gamma_2 \rho^0(\phi) \rightarrow \gamma_1 \gamma_2 \pi^+\pi^-(K^+K^-)$ can be expressed as

$$\begin{aligned} & \mathcal{M}(\phi_1, \theta_1, \phi_2, \theta_2, \phi_3, \theta_3; J, M, J_C, \lambda_1, \lambda_2, \lambda_3, \lambda_4) \\ &= B_{\lambda_1, \lambda_2}^J D_{M, \lambda_1 - \lambda_2}^{J\star}(\phi_1, \theta_1) A_{\lambda_3, \lambda_4}^{J_C} D_{\lambda_2, \lambda_3 - \lambda_4}^{J_C\star}(\phi_2, \theta_2) \\ & \quad \times F^1 D_{\lambda_4, 0}^{1\star}(\phi_3, \theta_3), \end{aligned} \quad (1)$$

where $B_{\lambda_1, \lambda_2}^J$ ("before" the χ_{cJ}) is the helicity amplitude of $\psi(2S) \rightarrow \gamma \chi_{cJ}$ decay, the superscript J is the spin of $\psi(2S)$ with $J = 1$, $A_{\lambda_3, \lambda_4}^{J_C}$ ("after" the χ_{cJ}) is the helicity amp-

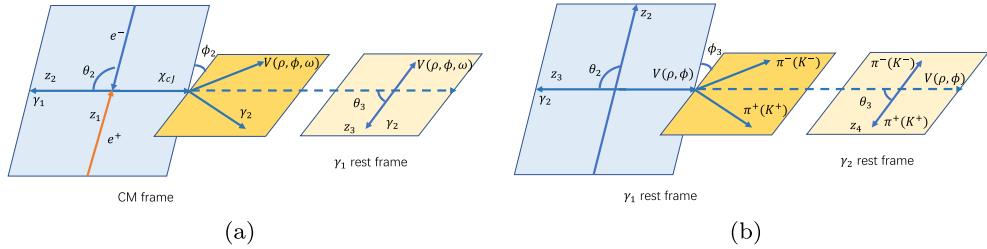


Fig. 1. (color online) Definition of helicity angles at e^+e^- collider experiment.

Table 2. Definition of helicity angles and amplitudes, where λ_i indicates the helicity and energy for the corresponding particles.

Decay Mode	Solid Angle	Helicity Amplitude
$\psi(2S)(\lambda_0) \rightarrow \gamma(\lambda_1)\chi_{cJ}(\lambda_2)$	$\Omega_1 = (\theta_1, \phi_1)$	$B_{\lambda_1, \lambda_2}^J$
$\chi_{cJ}(\lambda'_2) \rightarrow \gamma(\lambda_3)V(\lambda_4)$	$\Omega_2 = (\theta_2, \phi_2)$	$A_{\lambda_3, \lambda_4}^{Jc}$
$V(\lambda'_4) \rightarrow PP(\rho \rightarrow \pi^+\pi^-, \phi \rightarrow K^+K^-)$	$\Omega_3 = (\theta_3, \phi_3)$	F^1
$V(\lambda'_4) \rightarrow PPP(\omega \rightarrow \pi^+\pi^-\pi^0)$	$\Omega_3 = (\alpha, \beta, \gamma)$	F_0^1

litude of the process $\chi_{cJ} \rightarrow \gamma\rho^0(\chi_{cJ} \rightarrow \gamma\phi)$, the superscript Jc is the spin of χ_{cJ} and F^1 is the helicity amplitude of the decay $\rho^0 \rightarrow \pi^+\pi^-$ or $\phi \rightarrow K^+K^-$, respectively. The helicity amplitudes are subscripted by the helicity $\lambda_1 = \pm 1$ of the radiative photon from $\psi(2S) \rightarrow \gamma\chi_{cJ}$ decay, the helicity λ_2 ($\lambda_2 = 0$ for χ_{c0} , $\lambda_2 = 0, \pm 1$ for χ_{c1} and $\lambda_2 = 0, \pm 1, \pm 2$ for χ_{c2}) of χ_{cJ} , the helicity $\lambda_3 = \pm 1$ of the radiative photon from $\chi_{cJ} \rightarrow \gamma V(V = \rho^0, \phi)$, and the helicity $\lambda_4 = 0, \pm 1$ of the vector meson (ρ^0 or ϕ). The indices for the helicity of the daughters (psudoscalar mesons) from ρ^0 or ϕ decay can be omitted since they are zero. The subscript $M = \pm 1$ for the first Wigner D-function is z-component of spin J of $\psi(2S)$.

The total amplitude \mathcal{M} for the decay $\psi(2S) \rightarrow \gamma_1\chi_{cJ} \rightarrow \gamma_1\gamma_2\omega \rightarrow \gamma_1\gamma_2\pi^+\pi^-\pi^0$ is

$$\begin{aligned} & \mathcal{M}(\phi_1, \theta_1, \phi_2, \theta_2, \phi_3, \theta_3; J, M, Jc, \lambda_1, \lambda_2, \lambda_3, \lambda_4) \\ &= B_{\lambda_1, \lambda_2}^J D_{M, \lambda_1 - \lambda_2}^{J*}(\phi_1, \theta_1) A_{\lambda_3, \lambda_4}^{Jc} D_{\lambda_2, \lambda_3 - \lambda_4}^{Jc*}(\phi_2, \theta_2) \\ & \times F_\mu^1 D_{\lambda_4, \mu}^{1*}(\alpha, \beta, \gamma), \end{aligned} \quad (2)$$

where F_μ^1 is the helicity amplitude of the decay $\omega \rightarrow \pi^+\pi^-\pi^0$, respectively. And μ is the z-component of spin angular momentum J of ω , while the normal to the ω decay plane are taken as the z-axis. The symmetry relation requires only one amplitude $F_\mu^1(\mu = 0)$ [14].

The decay rates Γ for the cascade decays $\psi(2S) \rightarrow \gamma_1\chi_{cJ} \rightarrow \gamma_1\gamma_2\rho^0(\phi) \rightarrow \gamma_1\gamma_2\pi^+\pi^-(K^+K^-)$ and $\psi(2S) \rightarrow \gamma_1\chi_{cJ} \rightarrow \gamma_1\gamma_2\omega \rightarrow \gamma_1\gamma_2\pi^+\pi^-\pi^0$ are proportional to

$$\sum_{M, \lambda_1, \lambda_2, \lambda_3, \lambda_4} |\mathcal{M}(\phi_1, \theta_1, \phi_2, \theta_2, \phi_3, \theta_3; J, M, Jc, \lambda_1, \lambda_2, \lambda_3, \lambda_4)|^2. \quad (3)$$

The electromagnetic transitions $\psi(2S) \rightarrow \gamma\chi_{cJ}$ are dominant by electric dipole (E1) transitions, and its helicity amplitudes $B_{\lambda_1, \lambda_2}^J$ satisfy the E1 transition relations [15],

$$\begin{aligned} B_{1,1}^1 &= B_{1,0}^1 & \text{for } \psi(2S) \rightarrow \gamma_1\chi_{c1} \text{ decay,} \\ B_{1,2}^1 &= \sqrt{2}B_{1,1}^1 = \sqrt{6}B_{1,0}^1 & \text{for } \psi(2S) \rightarrow \gamma_1\chi_{c2} \text{ decay.} \end{aligned} \quad (4)$$

Parity conservation gives the relation $B_{\lambda_1, \lambda_2}^1 = B_{-\lambda_1, -\lambda_2}^1$

$\eta_{\psi(2S)}\eta_\gamma\eta_{\chi_{cJ}}(-1)^{s_{\psi(2S)} - s_\gamma - s_{\chi_{cJ}}}$, where η and s represents the parity and spin of the particle. So we have $B_{-1,0}^1 = B_{1,0}^1$ for the decay $\psi(2S) \rightarrow \gamma\chi_{c0}$, $B_{-1,-1}^1 = -B_{1,1}^1$, $B_{-1,0}^1 = -B_{1,0}^1$ for the decay $\psi(2S) \rightarrow \gamma\chi_{c1}$, and $B_{-1,-2}^1 = B_{1,2}^1$, $B_{-1,-1}^1 = -B_{1,1}^1$, $B_{-1,0}^1 = -B_{1,0}^1$ for the decay $\psi(2S) \rightarrow \gamma\chi_{c2}$. Angular momentum conservation $|\lambda_1 - \lambda_2| \leq 1$ requires that these amplitudes($B_{1,-1}^1, B_{-1,1}^1$) do not exist for the decay $\psi(2S) \rightarrow \gamma\chi_{c1}$, and $B_{1,-1}^1, B_{-1,1}^1, B_{-1,2}^1, B_{1,-2}^1$ do not exist for the decay $\psi(2S) \rightarrow \gamma\chi_{c2}$. The matrix of helicity amplitude can be written as

$$B = \begin{bmatrix} B_{-1,0}^1 \\ B_{0,0}^1 \\ B_{1,0}^1 \end{bmatrix} = \begin{bmatrix} B_{1,0}^1 \\ 0 \\ B_{1,0}^1 \end{bmatrix} \text{ for } \psi(2S) \rightarrow \gamma\chi_{c0} \text{ decay,} \quad (5)$$

$$\begin{aligned} B &= \begin{bmatrix} B_{-1,-1}^1 & B_{-1,0}^1 & 0 \\ B_{0,-1}^1 & B_{0,0}^1 & B_{0,1}^1 \\ 0 & B_{1,0}^1 & B_{1,1}^1 \end{bmatrix} = \begin{bmatrix} -B_{1,1}^1 & -B_{1,0}^1 & 0 \\ 0 & 0 & 0 \\ 0 & B_{1,0}^1 & B_{1,1}^1 \end{bmatrix} \\ &= \begin{bmatrix} -B_{1,0}^1 & -B_{1,0}^1 & 0 \\ 0 & 0 & 0 \\ 0 & B_{1,0}^1 & B_{1,0}^1 \end{bmatrix} \text{ for } \psi(2S) \rightarrow \gamma\chi_{c1} \text{ decay,} \end{aligned} \quad (6)$$

$$\begin{aligned} B &= \begin{bmatrix} B_{-1,-2}^1 & B_{-1,-1}^1 & B_{-1,0}^1 & B_{-1,1}^1 & 0 \\ B_{0,-2}^1 & B_{0,-1}^1 & B_{0,0}^1 & B_{0,1}^1 & B_{0,2}^1 \\ 0 & B_{1,-1}^1 & B_{1,0}^1 & B_{1,1}^1 & B_{1,2}^1 \end{bmatrix} \\ &= \begin{bmatrix} B_{1,2}^1 & B_{1,1}^1 & B_{1,0}^1 & 0 & 0 \\ 0 & 0 & 0 & 0 & 0 \\ 0 & 0 & B_{1,0}^1 & B_{1,1}^1 & B_{1,2}^1 \end{bmatrix} \text{ for } \psi(2S) \rightarrow \gamma\chi_{c2} \text{ decay.} \\ &= \begin{bmatrix} \sqrt{6}B_{1,0}^1 & \sqrt{3}B_{1,0}^1 & B_{1,0}^1 & 0 & 0 \\ 0 & 0 & 0 & 0 & 0 \\ 0 & 0 & B_{1,0}^1 & \sqrt{3}B_{1,0}^1 & \sqrt{6}B_{1,0}^1 \end{bmatrix} \end{aligned} \quad (7)$$

As for $\chi_{cJ} \rightarrow \gamma V(\rho^0, \phi, \omega)$ decays, only one independent helicity amplitude for χ_{c0} decays ($A_{1,1}^0$ or $A_{-1,-1}^0$, "so-called" transverse polarization amplitude A_{0V}^\perp in Ref. [16]), there are more than one independent helicity amplitudes for χ_{c1} and χ_{c2} decays. The helicity amplitudes can be expressed as $A_{\lambda_3, \lambda_4}^{Jc} = a_{\lambda_3, \lambda_4} * e^{i\zeta_{\lambda_3, \lambda_4}}$, where Jc is the spin of the mother particle, λ_i is the helicity value of daughter particles, a and ζ are the magnitude and phase angle of helicity amplitude A . Parity conservation leads to the following symmetry relations for helicity amplitudes as

$$\begin{aligned}
A_{1,1}^0 &= A_{-1,-1}^0 && \text{for } \chi_{c0} \text{ decay,} \\
A_{-1,-1}^1 &= -A_{1,1}^1, \quad A_{-1,0}^1 = -A_{1,0}^1 && \text{for } \chi_{c1} \text{ decay,} \\
A_{-1,-1}^2 &= A_{1,1}^2, \quad A_{-1,0}^2 = A_{1,0}^2, \quad A_{-1,1}^2 = A_{1,-1}^2 && \text{for } \chi_{c2} \text{ decay.}
\end{aligned} \tag{8}$$

We define a parameter for polarization observable to describe the relative magnitudes of two helicity amplitudes

$$x \equiv \frac{|A_{1,1}^1|}{|A_{1,0}^1|} = \frac{|A_{1V}^\perp|}{|A_{1V}^\parallel|} \tag{9}$$

for $\chi_{c1} \rightarrow \gamma V(\rho^0, \phi, \omega)$ decays, and two independent parameters

$$x \equiv \frac{|A_{1,1}^2|}{|A_{1,0}^2|} = \frac{|A_{2V}^\perp|}{|A_{2V}^\parallel|}, \quad y \equiv \frac{|A_{1,-1}^2|}{|A_{1,0}^2|} = \frac{|T_{2V}^\perp|}{|A_{2V}^\parallel|} \tag{10}$$

for $\chi_{c2} \rightarrow \gamma V(\rho, \phi, \omega)$ decays, where A or T with subscript \perp (transverse polarization) or \parallel (longitudinal polarization) is the amplitude defined in Ref. [16]. They have the significance of describing the ratio of amplitudes that characterize transverse polarization to longitudinal polarization.

The phase differences between independent amplitudes are defined as

$$\Delta_1 = \zeta_{1,0} - \zeta_{1,1} \tag{11}$$

for χ_{c1} , and

$$\Delta_1 = \zeta_{1,0} - \zeta_{1,1}, \quad \Delta_2 = \zeta_{1,-1} - \zeta_{1,1}, \tag{12}$$

for χ_{c2} .

III. SPIN DENSITY MATRIX

As one of the method to get the decay angular distributions, the spin density matrix (SDM) carries the dynamical information of particle decay, and its different parameterization can clearly explain various physical phenomena. For example, when expressed in multipole parameter form r_M^L (The L -rank index ranges from 1 to $2J$, M is taken from $-L$ to L), it can provide information about particle polarization [17, 18].

The spin density matrix of $\psi(2S)$ from polarized e^+e^- beams can be written to be

$$\rho^{\psi(2S)} = \frac{1}{2} \begin{bmatrix} (1 - \mathcal{P}_z)(1 + \bar{\mathcal{P}}_z) & 0 & P_T^2 \\ 0 & 0 & 0 \\ P_T^2 & 0 & (1 + \mathcal{P}_z)(1 - \bar{\mathcal{P}}_z) \end{bmatrix}, \tag{13}$$

where $\mathcal{P}_z/\bar{\mathcal{P}}_z$ is the degree of longitudinal polarization of e^+/e^- and P_T is the degree of transverse polarization of e^+/e^- [19].

By taking the direction of the photon's momentum as the positive z-axis direction as shown in Fig. 1(a), the SDM of χ_{c0} can be written as

$$\rho^{\chi_{c0}} = \frac{1}{2} b_{1,0}^2 (1 + \cos^2(\theta_1) + P_T^2 \sin^2(\theta_1) \cos(2\phi_1)), \tag{14}$$

while the matrix elements of $\rho^{\chi_{c1}}$ and $\rho^{\chi_{c2}}$ are listed in Append. 7, where $b_{1,0}$ is the magnitude of helicity amplitude $B_{1,0}$ in $\psi(2S) \rightarrow \gamma \chi_{cJ}$ decays. In these SDM calculations, we have used the E1 transition relations in the $\psi(2S) \rightarrow \gamma \chi_{cJ}$ decay [20].

In our paper, we take the multipole parameters r_M^L to describe the SDM of vectors ($V = \rho^0, \phi, \omega$), it is expressed as

$$\rho^V = \frac{r_0^0}{3} \begin{bmatrix} r_0^2 + \sqrt{3}r_0^1 + 1 & \sqrt{\frac{3}{2}}(-ir_{-1}^1 + r_1^1 - ir_{-1}^2 + r_1^2) & \sqrt{3}(r_2^2 - ir_{-2}^2) \\ \sqrt{\frac{3}{2}}(ir_{-1}^1 + r_1^1 + ir_{-1}^2 + r_1^2) & 1 - 2r_0^2 & \sqrt{\frac{3}{2}}(-ir_{-1}^1 + r_1^1 + ir_{-1}^2 - r_1^2) \\ \sqrt{3}(r_2^2 + ir_{-2}^2) & \sqrt{\frac{3}{2}}(ir_{-1}^1 + r_1^1 - ir_{-1}^2 - r_1^2) & r_0^2 - \sqrt{3}r_0^1 + 1 \end{bmatrix}. \tag{15}$$

In $\chi_{cJ} \rightarrow \gamma V(\rho, \phi, \omega)$ decays, the real multipole parameters r_M^L have different expressions for $J = 0, 1, 2$ as listed in Appendix B.

IV. JOINT ANGULAR DISTRIBUTION

In order to compare with experimental results from electron-positron collider, the joint angular distribution between the production and decay of χ_{cJ} is needed. The expressions of joint angular distribution can be obtained

easily using the SDMs of decay particles. Here we construct the joint angular distribution expressions for each decay level, which can be used experimentally to verify the measured results. The joint angular distributions for the processes $\psi(2S) \rightarrow \gamma_1 \chi_{cJ}$, $\psi(2S) \rightarrow \gamma_1 \chi_{cJ}, \chi_{cJ} \rightarrow \gamma_2 V (V = \rho^0, \phi, \omega)$ and $\psi(2S) \rightarrow \gamma_1 \chi_{cJ}, \chi_{cJ} \rightarrow \gamma_2 V (V = \rho^0, \phi, \omega)$, $V \rightarrow$ final states read

$$W(\Omega_1) \propto \text{Tr}[\rho^{\chi_{cJ}}], \tag{16}$$

$$\mathcal{W}(\Omega_1, \Omega_2) \propto \text{Tr}[\rho^V] = r_0^0, \quad (17)$$

$$\begin{aligned} \mathcal{W}(\Omega_1, \Omega_2, \Omega_3) &\propto \sum_{\lambda_4, \lambda'_4} \rho_{\lambda_4, \lambda'_4}^V D_{\lambda_4, 0}^{1*}(\Omega_3) D_{\lambda'_4, 0}^1(\Omega_3) |F_0^1|^2 \\ &\propto -\frac{1}{6} r_0^0 [2\sqrt{3} \sin^2 \theta_3 (r_{-2}^2 \sin 2\phi_3 \\ &\quad + r_2^2 \cos 2\phi_3) + 2\sqrt{3} \sin 2\theta_3 (r_{-1}^2 \sin \phi_3 \\ &\quad + r_1^2 \cos \phi_3) + 3r_0^2 \cos 2\theta_3 + r_0^2 - 2], \end{aligned} \quad (18)$$

respectively.

Taking into account the polarization observables used in experiment, we provide the distribution formulae for polar angle θ_i ($i = 1, 2, 3$) after integrating other polar angles and azimuthal angles.

For χ_{c0} ,

$$\frac{dN}{d\cos \theta_1} \propto 1 + \cos^2 \theta_1, \quad (19)$$

$$\frac{dN}{d\cos \theta_3} \propto 1 - \cos^2 \theta_3, \quad (20)$$

$$\begin{aligned} \frac{dN}{d\cos \theta_1 d\phi_1} &\propto 1 + \cos^2(\theta_1) \\ &\quad + Pt^2(1 - \cos^2(\theta_1)) \cos(2\phi_1) \end{aligned} \quad (21)$$

The angular distribution $dN/d\cos \theta_2$ is trivial due to the projection of the cosine polar angle $\cos \theta_2$ is flat.

For χ_{c1} ,

$$\frac{dN}{d\cos \theta_1} \propto 1 - \frac{1}{3} \cos^2 \theta_1, \quad (22)$$

$$\frac{dN}{d\cos \theta_2} \propto 1 + \frac{2x^2 - 1}{2x^2 + 3} \cos^2 \theta_2, \quad (23)$$

$$\frac{dN}{d\cos \theta_3} \propto 1 + \frac{2 - x^2}{x^2} \cos^2 \theta_3, \quad (24)$$

$$\begin{aligned} \frac{dN}{d\cos \theta_1 d\phi_1} &\propto 1 - \frac{1}{3} \cos^2(\theta_1) \\ &\quad - \frac{1}{3} Pt^2(1 - \cos^2(\theta_1)) \cos(2\phi_1). \end{aligned} \quad (25)$$

For χ_{c2} ,

$$\frac{dN}{d\cos \theta_1} \propto 1 + \frac{1}{13} \cos^2 \theta_1, \quad (26)$$

$$\frac{dN}{d\cos \theta_2} \propto 1 + \frac{-6x^2 + 6y^2 - 3}{10x^2 + 6y^2 + 9} \cos^2 \theta_2, \quad (27)$$

$$\frac{dN}{d\cos \theta_3} \propto 1 + \frac{2 - x^2 - y^2}{x^2 + y^2} \cos^2 \theta_3, \quad (28)$$

$$\begin{aligned} \frac{dN}{d\cos \theta_1 d\phi_1} &\propto 1 + \frac{1}{13} \cos^2 \theta_1 \\ &\quad + \frac{1}{13} Pt^2(1 - \cos^2(\theta_1)) \cos(2\phi_1) \end{aligned} \quad (29)$$

To validate the above angular distribution functions, MC simulation is performed with modeling by amplitude sampling of phase space events in Eqs. 3-12. The phase differences are naively set to be $\Delta_1 = \frac{\pi}{3}$ in χ_{c1} decays, and $\Delta_1 = \frac{\pi}{3}$ and $\Delta_2 = \frac{\pi}{4}$ in χ_{c2} decays. The degree of beam polarization is simply set to be $P_T = 0.24$ for all χ_{cJ} decays. The parameter x is set to be 0.43 for $\chi_{c1} \rightarrow \gamma\rho^0$ decay, 0.63 for $\chi_{c1} \rightarrow \gamma\phi$ decay, and 0.57 for $\chi_{c1} \rightarrow \gamma\omega$ decay, which is obtained from BESIII measurement in 2011 [7]. Referring to Ref. [20], the parameters for $\chi_{c2} \rightarrow \gamma V$ decays are arbitrarily chosen to be $x = 1.55$, $y = 2.06$ for $\chi_{c2} \rightarrow \gamma\rho^0$ decay, $x = 1.55$, $y = 2.13$ for $\chi_{c2} \rightarrow \gamma\phi$ decay, and $x = 0$, $y = 1$ for $\chi_{c2} \rightarrow \gamma\omega$ decay, respectively. 500,000 pseudoexperiments for each decay mode are generated and fitted using a probability density function derived from the full angular distributions shown in Eqs 19-29.

Here we list some fit results, and the others can be found in Appendix. C. We use the function $1 + \alpha \cos^2 \theta$ to fit the angular distributions of $\psi(2S) \rightarrow \gamma\chi_{cJ}$ ($J = 0, 1, 2$) in Eq. 19, 22, 26 and $\rho^0 \rightarrow \pi^+ \pi^-$, $\phi \rightarrow K^+ K^-$, $\omega \rightarrow \pi^+ \pi^- \pi^0$ from $\chi_{c0} \rightarrow \gamma V$ ($V = \rho^0, \phi, \omega$) decays in Eq. 21. In the case, the fitted α values are 0.992 ± 0.009 for the decay $\psi(2S) \rightarrow \gamma\chi_{c0}$ and -0.999 ± 0.001 for the decay $\phi \rightarrow K^+ K^-$ from $\chi_{c0} \rightarrow \gamma\phi$ decay in Fig. 8(a) and Fig. 8(b), respectively, which are consistent with the default values in Eq. 19 and Eq. 21 within the standard deviation. With the measured angular distributions of $\chi_{cJ} \rightarrow \gamma V$ ($J = 0, 1, 2$), we can extract the parameter $\hat{x}(x, y, P_T)$ in χ_{cJ} decays by fitting these equations of joint angular distributions to data. Given an example for fitting the angular distributions of $\chi_{cJ} \rightarrow \gamma\phi$ ($J = 1, 2$) based on MC simulation samples, the fitted x and P_T value in $\chi_{c1} \rightarrow \gamma\phi$ decays are 0.630 ± 0.002 and 0.26 ± 0.02 in Fig. 3(b), Fig. 3(c) and Fig. 3(d), which are in agreement with the input $x = 0.63$ and $P_T = 0.24$. In $\chi_{c2} \rightarrow \gamma\phi$ decays, the fitted parameters of x and y are $x = 1.558 \pm 0.344$, $y = 2.137 \pm 0.251$ in Fig. 4(b) and Fig. 4(c), respectively, which are consistent with the input $x = 1.55$, $y = 2.13$.

V. SENSITIVITY ESTIMATION

By investigating the statistical sensitivity of specific

parameters, the precise measurement is beneficial from evaluating the potential impact of uncertainties on the final results. The estimation aims to enhance the understanding of the experimental uncertainties associated with these parameters and observed signal yields. It is necessary to estimate the sensitivity in order to guide the data acquisition plan for the large-scale e^+e^- experimental devices, which are operating currently like BEPCII, and to be built in the future, such as Super-Tau Charm Facility (STCF) [21, 22]. Through rigorous statistical analysis and simulations, the research provides valuable insights into the sensitivity of key parameters, enabling researchers to make informed decisions and draw meaningful conclusions from the experimental data.

Assuming that the parameters will be obtained by fitting to the maximum likelihood function event by event, then the normalized joint angular distribution is defined as

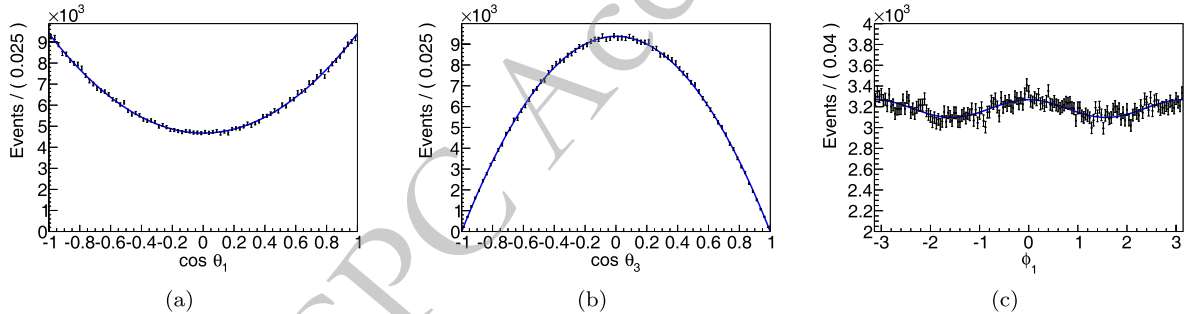


Fig. 2. (color online) Fits to the angular distributions of $\cos\theta_1$, ϕ_1 in $\psi(2S) \rightarrow \gamma\chi_{c0}$ and $\cos\theta_3$ in $\phi \rightarrow K^+K^-$ from $\chi_{c0} \rightarrow \gamma\phi$ decays. Dots with error bars represent MC events, and the blue solid curve denotes the fit.

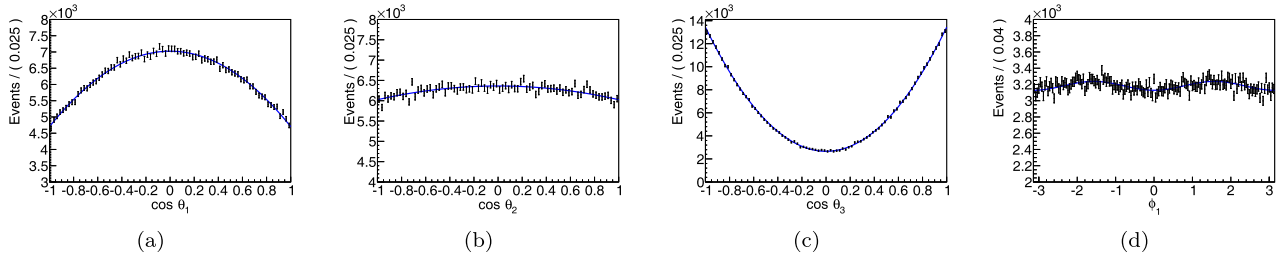


Fig. 3. (color online) Fits to the angular distributions of $\cos\theta_i$ ($i = 1, 2, 3$) and ϕ_1 in $\psi(2S) \rightarrow \gamma\chi_{c1}$, $\chi_{c1} \rightarrow \gamma\phi$ and $\phi \rightarrow K^+K^-$ decays. Dots with error bars represent MC events, and the blue solid curve denotes the fit.

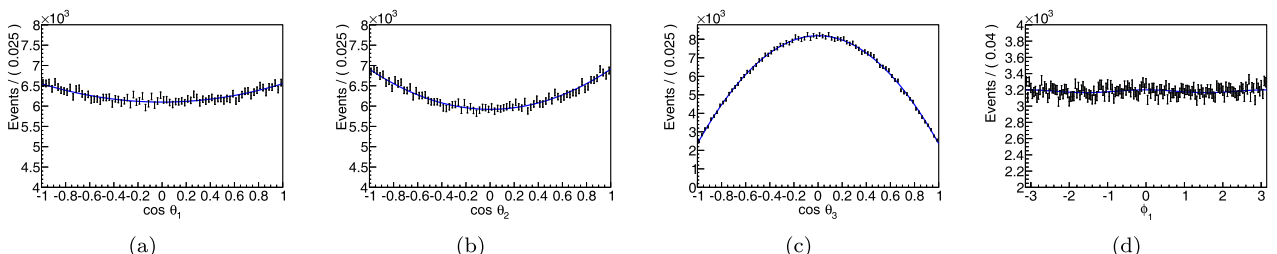


Fig. 4. (color online) Fits to the angular distributions of $\cos\theta_i$ ($i = 1, 2, 3$) and ϕ_1 in $\psi(2S) \rightarrow \gamma\chi_{c2}$, $\chi_{c2} \rightarrow \gamma\phi$ and $\phi \rightarrow K^+K^-$ decays. Dots with error bars represent MC events, and the blue solid curve denotes the fit.

where the covariance matrix gives

$$\begin{aligned} V_{x_i, x_j}^{-1} &= E\left[-\frac{\partial^2 \ln L}{\partial x_i \partial x_j}\right] \\ &= N \int -\widetilde{W} \cdot \left(\frac{\partial^2 \ln \widetilde{W}}{\partial x_i \partial x_j}\right) \prod_{k=1}^3 d\cos\theta_k \prod_{l=1}^3 d\phi_l. \end{aligned} \quad (33)$$

By taking the phase difference $\Delta_1 = \frac{\pi}{3}$ in χ_{c1} decays, the dependence of the statistical sensitivity for a set of different x value is plotting in Fig. 6(a). In χ_{c2} decays, the three phase differences Δ_1 and Δ_2 are set to be $\frac{\pi}{3}$ and $\frac{\pi}{4}$, respectively. The parameter $y(x)$ is set to be 1 in plotting the dependence of the statistical sensitivity for a set of different $x(y)$ in Fig. 7(a) and Fig. 7(b).

From Fig. 5, Fig. 6(b) and Fig. 7(c), we can see that with the increase in polarization, the number of events required under the same statistical significance decreases. In Fig. 6(a), we can see that the ratio of the two independent helicity amplitude modulus x in χ_{c1} decays can be measured at a statistical sensitivity to an order of 1% with at least 20,000 observed signal yields, where background, detector acceptance, and other experimental effects are not taken into account, if assuming $x = 1$. In comparison to the decay of χ_{c1} , the decay of χ_{c2} involves two independent parameters x and y , necessitating a higher num-

ber of observed events to achieve the same statistical sensitivity in the measurement of these two parameters.

The expected number of observed signal yields for the processes $\psi(2S) \rightarrow \gamma_1 \chi_{c1,2} \rightarrow \gamma_1 \gamma_2 \rho^0 \rightarrow \gamma_1 \gamma_2 \pi^+ \pi^-$, $\psi(2S) \rightarrow \gamma_1 \chi_{c1,2} \rightarrow \gamma_1 \gamma_2 \phi \rightarrow \gamma_1 \gamma_2 K^+ K^-$ and $\psi(2S) \rightarrow \gamma_1 \chi_{cJ} \rightarrow \gamma_1 \gamma_2 \omega \rightarrow \gamma_1 \gamma_2 \pi^+ \pi^- \pi^0$ are calculated by using the following equation:

where N_{sig} represents the expected number of observed signal events, $N_{\psi(2S)}$ represents the total number of $\psi(2S)$ data samples at BESIII or STCF, and ϵ is the expected experimental reconstruction efficiency. Additinally,

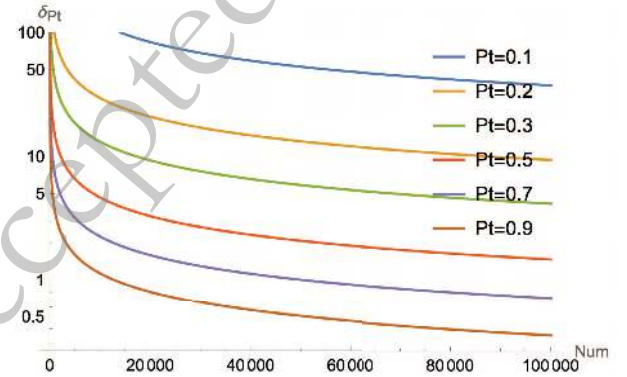
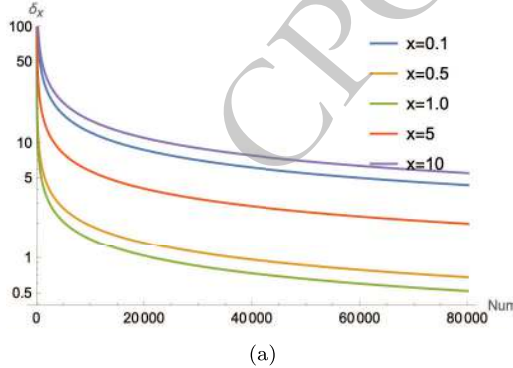
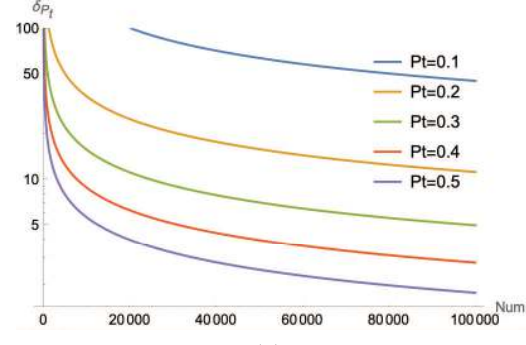


Fig. 5. (color online) The sensitivity of P_T (in χ_{c0} decay) for different P_T values relative to the observed events N

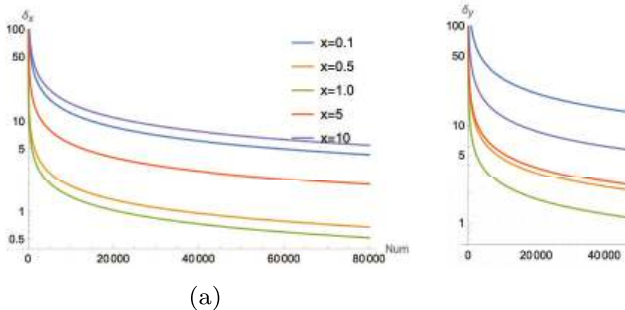


(a)

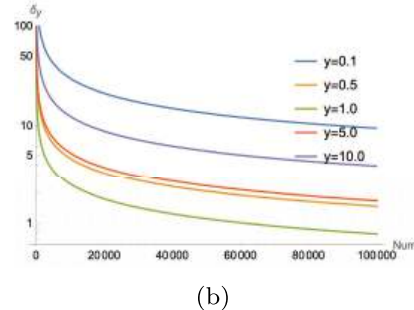


(b)

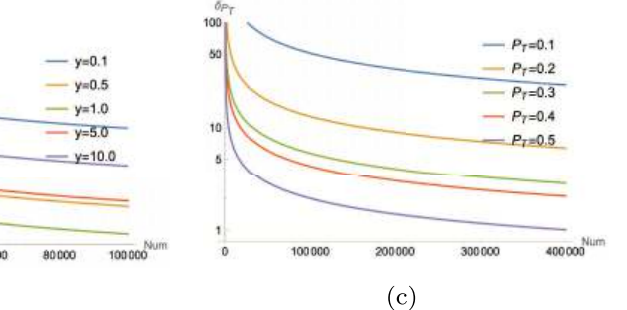
Fig. 6. (color online) (a) The sensitivity of x (in χ_{c1} decay) for different x values relative to the observed events N . (b) The sensitivity of P_T (in χ_{c1} decay) for different P_T values relative to the observed events N



(a)



(b)



(c)

Fig. 7. (color online) (a) The sensitivity of x (in χ_{c2} decay) for different x values relative to the observed events N . (b) The sensitivity of y (in χ_{c2} decay) for different y values relative to the observed events N . (c) The sensitivity of P_T (in χ_{c2} decay) for different P_T values relative to the observed events N .

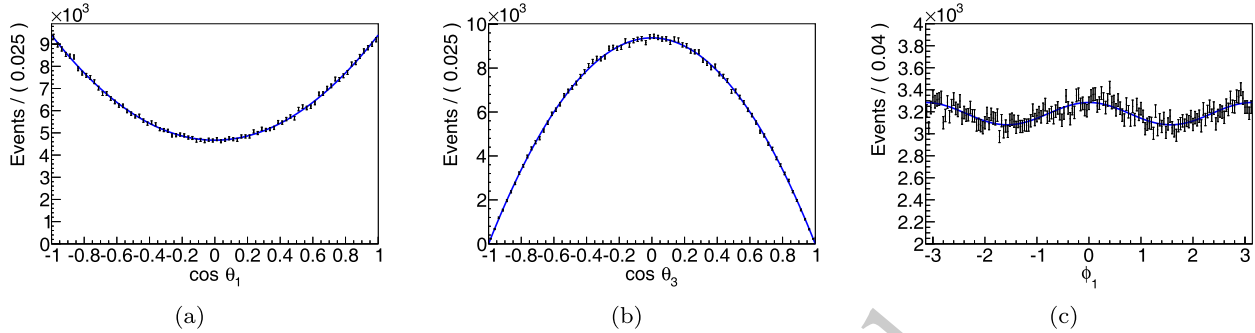


Fig. 8. (color online) $dN/d\cos\theta_1$, $dN/d\cos\theta_3$ and $dN/d\phi_1$ distributions versus $\cos\theta_1$, $\cos\theta_3$ and ϕ_1 in $\psi(2S)\rightarrow\gamma\chi_{c0}$ and $\omega\rightarrow\pi^+\pi^-\pi^0$ from $\chi_{c0}\rightarrow\gamma\omega$ decays. Dots with error bars are filled with MC events, and the blue solid curve denotes the fit.

$Br_{\psi(2S)\rightarrow\gamma\chi_{cJ}}$, $Br_{\chi_{cJ}\rightarrow\gamma_2V}$ and $Br_{V\rightarrow final\,states}$ denote the branching ratio of $\psi(2S)\rightarrow\gamma_1\chi_{cJ}$ ($J=0,1,2$), $\chi_{cJ}\rightarrow\gamma_2V(V=\rho^0, \phi, \omega)$ and $\rho^0\rightarrow\pi^+\pi^- \mid \phi\rightarrow K^+K^- \mid \omega\rightarrow\pi^+\pi^-\pi^0$, respectively. BESIII has collected about 2.71 billion (B) $\psi(2S)$ events in 2009, 2012 and 2021, and plan to collect 3 billion (B) $\psi(2S)$ events [21]. The future high-luminosity e^+e^- collider STCF will collect approximately 640 billion (B) $\psi(2S)$ data samples each year [22]. In Table 3, we obtain the expected number of observed signal yields for the processes $\psi(2S)\rightarrow\gamma_1\chi_{c0,1,2}, \chi_{c0,1,2}\rightarrow\gamma_2V(V=\rho^0, \phi, \omega)$ based on 2.71 B $\psi(2S)$ data samples at BESIII and 640 B $\psi(2S)$ data samples at STCF. With the expected signal yields, we can estimate the statistical sensitivity of the relative mag-

nitudes of transverse to longitudinal polarization amplitudes δ_x (δ_y, δ_{P_T}) for the processes $\psi(2S)\rightarrow\gamma_1\chi_{c0,1,2}\rightarrow\gamma_1\gamma_2V(V=\rho^0, \phi, \omega)$ based on 2.71 B and 640 B $\psi(2S)$ events in Table 4. The results of δ_{P_T} indicate that the degree of beam transverse polarization has a large statistical uncertainty based on current data. The statistical sensitivity δ_x is 1.4%–4.3% for $\chi_{c1}\rightarrow\gamma V$ decays with 2.71 B $\psi(2S)$ data samples in current BESIII experiment, which reaches at least 5-fold improvement over BESIII measurement in 2011 with $(1.06\pm 0.04)\times 10^8$ $\psi(2S)$ data samples [7]. The processes $\chi_{c2}\rightarrow\gamma V$ is promising to be observed at BESIII, and its statistical sensitivity δ_x and δ_y are conservatively estimated to be up to the levels of 10–20% based on 2.71 B $\psi(2S)$ data samples. The STCF

Table 3. The expected number of observed signal events and the related parameters for calculating the expected signal yields for the processes $\psi(2S)\rightarrow\gamma_1\chi_{c0,1,2}\rightarrow\gamma_1\gamma_2V(V=\rho^0, \phi, \omega)$ at BESIII and STCF experiment. The upper limits for $\chi_{c2}\rightarrow\gamma V$ are at 90% C.L..

N_{sig}	$N_{\Psi(2S)}$	$Br_{\psi(2S)\rightarrow\gamma_1\chi_{cJ}} (\%)$ [1]	$Br_{\chi_{cJ}\rightarrow\gamma_2V} (10^{-5})$ [1]	$Br_{V\rightarrow final\,states} (\%)$ [1]	$\epsilon (\%)$ [7]
537			$<0.9 (\chi_{c0}\rightarrow\gamma\rho^0)$	$100 (\rho^0\rightarrow\pi^+\pi^-)$	22.6
253		9.77 ($\psi(2S)\rightarrow\gamma\chi_{c0}$)	$<0.6 (\chi_{c0}\rightarrow\gamma\phi)$	$49.1 (\phi\rightarrow K^+K^-)$	32.4
337			$<0.8 (\chi_{c0}\rightarrow\gamma\omega)$	$89.2 (\omega\rightarrow\pi^+\pi^-\pi^0)$	18.6
11072			$21.6 (\chi_{c1}\rightarrow\gamma\rho^0)$	$100 (\rho^0\rightarrow\pi^+\pi^-)$	19.4
1080	2.71×10^9 (BESIII)	9.75 ($\psi(2S)\rightarrow\gamma\chi_{c1}$)	$2.4 (\chi_{c1}\rightarrow\gamma\phi)$	$49.1 (\phi\rightarrow K^+K^-)$	34.6
3493			$6.8 (\chi_{c1}\rightarrow\gamma\omega)$	$89.2 (\omega\rightarrow\pi^+\pi^-\pi^0)$	22.7
788			$<1.9 (\chi_{c2}\rightarrow\gamma\rho^0)$	$100 (\rho^0\rightarrow\pi^+\pi^-)$	15.7
339		9.36 ($\psi(2S)\rightarrow\gamma\chi_{c2}$)	$<0.8 (\chi_{c2}\rightarrow\gamma\phi)$	$49.1 (\phi\rightarrow K^+K^-)$	32.6
261			$<0.6 (\chi_{c2}\rightarrow\gamma\omega)$	$89.2 (\omega\rightarrow\pi^+\pi^-\pi^0)$	19.2
1.27×10^5			$<0.9 (\chi_{c0}\rightarrow\gamma\rho^0)$	$100 (\rho^0\rightarrow\pi^+\pi^-)$	22.6
5.97×10^4		9.77 ($\psi(2S)\rightarrow\gamma\chi_{c0}$)	$<0.6 (\chi_{c0}\rightarrow\gamma\phi)$	$49.1 (\phi\rightarrow K^+K^-)$	32.4
7.95×10^4			$<0.8 (\chi_{c0}\rightarrow\gamma\omega)$	$89.2 (\omega\rightarrow\pi^+\pi^-\pi^0)$	18.6
2.61×10^6			$21.6 (\chi_{c1}\rightarrow\gamma\rho^0)$	$100 (\rho^0\rightarrow\pi^+\pi^-)$	19.4
2.55×10^5	6.4×10^{11} (STCF)	9.75 ($\psi(2S)\rightarrow\gamma\chi_{c1}$)	$2.4 (\chi_{c1}\rightarrow\gamma\phi)$	$49.1 (\phi\rightarrow K^+K^-)$	34.6
8.25×10^5			$6.8 (\chi_{c1}\rightarrow\gamma\omega)$	$89.2 (\omega\rightarrow\pi^+\pi^-\pi^0)$	22.7
1.86×10^5			$<1.9 (\chi_{c2}\rightarrow\gamma\rho^0)$	$100 (\rho^0\rightarrow\pi^+\pi^-)$	15.7
8.01×10^4		9.36 ($\psi(2S)\rightarrow\gamma\chi_{c2}$)	$<0.8 (\chi_{c2}\rightarrow\gamma\phi)$	$49.1 (\phi\rightarrow K^+K^-)$	32.6
6.16×10^4			$<0.6 (\chi_{c2}\rightarrow\gamma\omega)$	$89.2 (\omega\rightarrow\pi^+\pi^-\pi^0)$	19.2

Table 4. The statistical sensitivity δ_x (δ_y , δ_{P_T}) for the processes $\psi(2S) \rightarrow \gamma_1 \chi_{c0,1,2} \rightarrow \gamma_1 \gamma_2 V (V = \rho^0, \phi, \omega)$ based on 2.71 billion $\Psi(2S)$ events at BESIII and 640 billion $\Psi(2S)$ events at STCF.

Decay Mode	Parameter	Input value	δ_x (2.71B)	δ_y (2.71B)	δ_{P_T} (2.71B)	δ_x (640B)	δ_y (640B)	δ_{P_T} (640B)
$\chi_{c0} \rightarrow \gamma \rho^0$	P_T	0.2	—	—	—	7.69%	—	—
$\chi_{c0} \rightarrow \gamma \phi$	P_T	0.2	—	—	—	7.27%	—	—
$\chi_{c0} \rightarrow \gamma \omega$	P_T	0.2	—	—	—	8.27%	—	—
	x	1						
$\chi_{c1} \rightarrow \gamma \rho^0$	P_T	0.2 (fixed)	1.4%	—	32.5%	0.1%	—	2.1%
	Δ_1	$\frac{\pi}{3}$ (fixed)						
	x	1						
$\chi_{c1} \rightarrow \gamma \phi$	P_T	0.2 (fixed)	4.3%	—	—	0.3%	—	6.8%
	Δ_1	$\frac{\pi}{3}$ (fixed)						
	x	1						
$\chi_{c1} \rightarrow \gamma \omega$	P_T	0.2 (fixed)	2.4%	—	59.1%	0.2%	—	3.8%
	Δ_1	$\frac{\pi}{3}$ (fixed)						
	x	1						
	y	1						
$\chi_{c2} \rightarrow \gamma \rho^0$	P_T	0.2 (fixed)	8.6%	8.4%	—	0.6%	0.5%	9.0%
	Δ_1	$\frac{\pi}{3}$ (fixed)						
	Δ_2	$\frac{\pi}{4}$ (fixed)						
	x	1						
	y	1						
$\chi_{c2} \rightarrow \gamma \phi$	P_T	0.2 (fixed)	13.7%	13.3%	—	0.9%	0.9%	14.2%
	Δ_1	$\frac{\pi}{3}$ (fixed)						
	Δ_2	$\frac{\pi}{4}$ (fixed)						
	x	1						
	y	1						
$\chi_{c2} \rightarrow \gamma \omega$	P_T	0.2 (fixed)	15.6%	15.1%	—	1.0%	1.0%	16.2%
	Δ_1	$\frac{\pi}{3}$ (fixed)						
	Δ_2	$\frac{\pi}{4}$ (fixed)						

experiment is expected to further improve the sensitivity δ_x for χ_{c1} decays and δ_x , δ_y for χ_{c2} decays with an impressive precision less than or equal to 1% based the 640 B $\psi(2S)$ data sample, presenting the improvement of 1 order of magnitude compare to BESIII experiment with 2.71 B $\psi(2S)$ data samples. The sensitivity δ_{P_T} for χ_{c1} and χ_{c2} decays ranges from 2% to 20% at STCF experiment.

$$N_{\text{sig}} = N_{\Psi(2S)} \times Br_{\psi(2S) \rightarrow \gamma_1 \chi_{cJ}} \times Br_{\chi_{cJ} \rightarrow \gamma_2 V} \times Br_{V \rightarrow \text{final states}} \times \epsilon, \quad (34)$$

VI. SUMMARY AND OUTLOOK

To better understand the radiative decays of $\psi(2S) \rightarrow \gamma \chi_{cJ}, \chi_{cJ} \rightarrow \gamma V (\rho^0, \phi, \omega)$, we present formulae of helicity amplitude analysis and derive the joint angular distribution for these decay chains. Furthermore, we provide observables for experimentally measuring the polarization of the vector mesons in χ_{cJ} decays, perform the Monte Carlo simulation and fit the angular distributions to validate the theoretical calculations. Finally, we investigate the statistical sensitivity of the degree of transverse polarization P_T of $e^+ e^-$ beams and the modulus ratio of

helicity amplitudes in the decays of χ_{c1} and χ_{c2} , and predict the expected number of signal events required to achieve the relevant statistical precision in experimental measurements. Based on 3 billion $\psi(2S)$ planned data samples at BESIII experiment, the ratio of transverse to longitudinal polarization amplitude for the process $\chi_{cJ} \rightarrow \gamma V(\rho, \phi, \omega)$ can be measured in the near future [21]. The formalism in the work can be used for near future re-

search in high-energy physics experiments like STCF with 640 billion $\psi(2S)$ data samples per year [22]. Analogous to the radiative decay of a charmonium state with the same spin-parity quantum number, it also provides a reference for future measurements on the super-B factory to study the polarization effect of P-wave bottomonia $\chi_{bJ} \rightarrow \gamma V(\rho^0, \phi, \omega)$ [24].

APPENDIX A: THE SPIN DENSITY MATRIX ELEMENTS OF χ_{c1} AND χ_{c2}

A.1. The spin density matrix elements of χ_{c1}

$$\begin{aligned}
\rho_{1,1}^{\chi_{c1}} &= -\frac{1}{2} b_{1,0}^2 \sin^2(\theta_1) (P_T^2 \cos(2\phi_1) - 1), \\
\rho_{1,0}^{\chi_{c1}} &= \frac{b_{1,0}^2 \sin(\theta_1) (\cos(\theta_1) (P_T^2 \cos(2\phi_1) - 1) - iP_T^2 \sin(2\phi_1))}{2\sqrt{2}}, \\
\rho_{0,1}^{\chi_{c1}} &= \frac{b_{1,0}^2 \sin(\theta_1) (\cos(\theta_1) (P_T^2 \cos(2\phi_1) - 1) + iP_T^2 \sin(2\phi_1))}{2\sqrt{2}}, \\
\rho_{0,0}^{\chi_{c1}} &= \frac{1}{4} b_{1,0}^2 (\cos(2\theta_1) + 2P_T^2 \sin^2(\theta_1) \cos(2\phi_1) + 3), \\
\rho_{0,-1}^{\chi_{c1}} &= \frac{b_{1,0}^2 \sin(\theta_1) (\cos(\theta_1) (1 - P_T^2 \cos(2\phi_1)) + iP_T^2 \sin(2\phi_1))}{2\sqrt{2}}, \\
\rho_{-1,0}^{\chi_{c1}} &= -\frac{b_{1,0}^2 \sin(\theta_1) (\cos(\theta_1) (P_T^2 \cos(2\phi_1) - 1) + iP_T^2 \sin(2\phi_1))}{2\sqrt{2}}, \\
\rho_{-1,-1}^{\chi_{c1}} &= -\frac{1}{2} b_{1,0}^2 \sin^2(\theta_1) (P_T^2 \cos(2\phi_1) - 1), \\
\rho_{1,-1}^{\chi_{c1}} &= \rho_{-1,1}^{\chi_{c1}} = 0.
\end{aligned} \tag{A1}$$

A.2. The spin density matrix elements of χ_{c2}

$$\begin{aligned}
\rho_{2,2}^{\chi_{c2}} &= \frac{3}{4} b_{1,0}^2 (\cos(2\theta_1) + 2P_T^2 \sin^2(\theta_1) \cos(2\phi_1) + 3), \\
\rho_{2,1}^{\chi_{c2}} &= \frac{3}{2} b_{1,0}^2 \sin(\theta_1) (\cos(\theta_1) (1 - P_T^2 \cos(2\phi_1)) + iP_T^2 \sin(2\phi_1)), \\
\rho_{2,0}^{\chi_{c2}} &= \frac{1}{4} \sqrt{\frac{3}{2}} b_{1,0}^2 (2 \sin^2(\theta_1) + P_T^2 ((\cos(2\theta_1) + 3) \cos(2\phi_1) - 4i \cos(\theta_1) \sin(2\phi_1))), \\
\rho_{1,2}^{\chi_{c2}} &= \frac{1}{2} (-3) b_{1,0}^2 \sin(\theta_1) (\cos(\theta_1) (P_T^2 \cos(2\phi_1) - 1) + iP_T^2 \sin(2\phi_1)), \\
\rho_{1,1}^{\chi_{c2}} &= \frac{1}{2} (-3) b_{1,0}^2 \sin^2(\theta_1) (P_T^2 \cos(2\phi_1) - 1), \\
\rho_{1,0}^{\chi_{c2}} &= \frac{1}{2} \sqrt{\frac{3}{2}} b_{1,0}^2 \sin(\theta_1) (\cos(\theta_1) (P_T^2 \cos(2\phi_1) - 1) - iP_T^2 \sin(2\phi_1)), \\
\rho_{0,2}^{\chi_{c2}} &= \frac{1}{4} \sqrt{\frac{3}{2}} b_{1,0}^2 (2 \sin^2(\theta_1) + P_T^2 ((\cos(2\theta_1) + 3) \cos(2\phi_1) + 4i \cos(\theta_1) \sin(2\phi_1))), \\
\rho_{0,1}^{\chi_{c2}} &= \frac{1}{2} \sqrt{\frac{3}{2}} b_{1,0}^2 \sin(\theta_1) (\cos(\theta_1) (P_T^2 \cos(2\phi_1) - 1) + iP_T^2 \sin(2\phi_1)),
\end{aligned}$$

$$\begin{aligned}
\rho_{0,0}^{\chi_{c2}} &= \frac{1}{4} b_{1,0}^2 (\cos(2\theta_1) + 2P_T^2 \sin^2(\theta_1) \cos(2\phi_1) + 3), \\
\rho_{0,-1}^{\chi_{c2}} &= \frac{1}{2} \sqrt{\frac{3}{2}} b_{1,0}^2 \sin(\theta_1) (\cos(\theta_1) (1 - P_T^2 \cos(2\phi_1)) + iP_T^2 \sin(2\phi_1)), \\
\rho_{0,-2}^{\chi_{c2}} &= \frac{1}{4} \sqrt{\frac{3}{2}} b_{1,0}^2 (2 \sin^2(\theta_1) + P_T^2 ((\cos(2\theta_1) + 3) \cos(2\phi_1) - 4i \cos(\theta_1) \sin(2\phi_1))), \\
\rho_{-1,0}^{\chi_{c2}} &= -\frac{1}{2} \sqrt{\frac{3}{2}} b_{1,0}^2 \sin(\theta_1) (\cos(\theta_1) (P_T^2 \cos(2\phi_1) - 1) + iP_T^2 \sin(2\phi_1)), \\
\rho_{-1,-1}^{\chi_{c2}} &= \frac{1}{2} (-3) b_{1,0}^2 \sin^2(\theta_1) (P_T^2 \cos(2\phi_1) - 1), \\
\rho_{-1,-2}^{\chi_{c2}} &= \frac{3}{2} b_{1,0}^2 \sin(\theta_1) (\cos(\theta_1) (P_T^2 \cos(2\phi_1) - 1) - iP_T^2 \sin(2\phi_1)), \\
\rho_{-2,0}^{\chi_{c2}} &= \frac{1}{4} \sqrt{\frac{3}{2}} b_{1,0}^2 (2 \sin^2(\theta_1) + P_T^2 ((\cos(2\theta_1) + 3) \cos(2\phi_1) + 4i \cos(\theta_1) \sin(2\phi_1))), \\
\rho_{-2,-1}^{\chi_{c2}} &= \frac{3}{2} b_{1,0}^2 \sin(\theta_1) (\cos(\theta_1) (P_T^2 \cos(2\phi_1) - 1) + iP_T^2 \sin(2\phi_1)), \\
\rho_{-2,-2}^{\chi_{c2}} &= \frac{3}{4} b_{1,0}^2 (\cos(2\theta_1) + 2P_T^2 \sin^2(\theta_1) \cos(2\phi_1) + 3), \\
\rho_{2,-1}^{\chi_{c2}} = \rho_{2,-2}^{\chi_{c2}} = \rho_{1,-1}^{\chi_{c2}} = \rho_{1,-2}^{\chi_{c2}} = \rho_{-1,2}^{\chi_{c2}} = \rho_{-1,1}^{\chi_{c2}} = \rho_{-2,1}^{\chi_{c2}} = \rho_{-2,2}^{\chi_{c2}} &= 0
\end{aligned} \tag{A2}$$

B. r_M^L expressions

B.1. χ_{c0}

The multipole parameters r_M^L for χ_{c0} are expressed as

$$r_0^0 = a_{1,1}^2 b_{1,0}^2 (1 + \cos^2(\theta_1) + P_T^2 \sin^2(\theta_1) \cos(2\phi_1)), r_0^0 r_0^2 = \frac{1}{2} a_{1,1}^2 b_{1,0}^2 (1 + \cos^2(\theta_1) + P_T^2 \sin^2(\theta_1) \cos(2\phi_1)). \tag{B1}$$

The other r_M^L unlisted are equal to zero.

B.2. χ_{c1}

The multipole parameters r_M^L for χ_{c1} are expressed as

$$\begin{aligned}
r_0^0 &= \frac{1}{12} a_{1,0}^2 b_{1,0}^2 (-3 \sin(2\theta_1) \sin(2\theta_2) \cos(\phi_2) + 6P_T^2 (1 - 2x^2) \sin(\theta_1) \sin(2\theta_2) \sin(2\phi_1) \sin(\phi_2) \\
&\quad + 6P_T^2 \sin^2(\theta_1) \cos(2\phi_1) ((2x^2 - 1) \cos(2\theta_2) - 1) + 3 \sin(2\theta_1) \sin(2\theta_2) \cos(\phi_2) (P_T^2 (1 - 2x^2) \cos(2\phi_1) + 2x^2) \\
&\quad + 2(2x^2 - 1) \cos^2(\theta_1) (3 \cos(2\theta_2) + 1) - 2(x^2 + 1) \cos(2\theta_1) + 10x^2 + 10), \\
r_0^0 r_{-1}^1 &= \frac{1}{4} \sqrt{3} x a_{1,0}^2 b_{1,0}^2 \sin(\Delta_1) (2 \sin(2\theta_2) (\cos^2(\theta_1) + P_T^2 \sin^2(\theta_1) \cos(2\phi_1)) \\
&\quad + \cos(2\theta_2) (2P_T^2 \sin(\theta_1) \sin(2\phi_1) \sin(\phi_2) + \sin(2\theta_1) \cos(\phi_2) (P_T^2 \cos(2\phi_1) - 1))), \\
r_0^0 r_1^1 &= \frac{1}{4} \sqrt{3} x a_{1,0}^2 b_{1,0}^2 \sin(\Delta_1) \cos(\theta_2) (2P_T^2 \sin(\theta_1) \sin(2\phi_1) \cos(\phi_2) + \sin(2\theta_1) \sin(\phi_2) (1 - P_T^2 \cos(2\phi_1))), \\
r_0^0 r_{-1}^2 &= \frac{1}{4} \sqrt{3} x a_{1,0}^2 b_{1,0}^2 \cos(\Delta_1) \cos(\theta_2) (\sin(2\theta_1) \sin(\phi_2) (P_T^2 \cos(2\phi_1) - 1) - 2P_T^2 \sin(\theta_1) \sin(2\phi_1) \cos(\phi_2)), \\
r_0^0 r_0^2 &= \frac{1}{12} a_{1,0}^2 b_{1,0}^2 (3 \sin(2\theta_1) \sin(2\theta_2) \cos(\phi_2) - 6P_T^2 (x^2 + 1) \sin(\theta_1) \sin(2\theta_2) \sin(2\phi_1) \sin(\phi_2) \\
&\quad + 6P_T^2 \sin^2(\theta_1) \cos(2\phi_1) ((x^2 + 1) \cos(2\theta_2) + 1) - 3 \sin(2\theta_1) \sin(2\theta_2) \cos(\phi_2) (P_T^2 (x^2 + 1) \cos(2\phi_1) - x^2) \\
&\quad + 2(x^2 + 1) \cos^2(\theta_1) (3 \cos(2\theta_2) + 1) - (x^2 - 2) \cos(2\theta_1) + 5x^2 - 10),
\end{aligned}$$

$$\begin{aligned} r_0^0 r_1^2 &= \frac{1}{4} \sqrt{3} x a_{1,0}^2 b_{1,0}^2 \cos(\Delta_1) (2 \sin(2\theta_2) (\cos^2(\theta_1) + P_T^2 \sin^2(\theta_1) \cos(2\phi_1)) \\ &\quad + \cos(2\theta_2) (2P_T^2 \sin(\theta_1) \sin(2\phi_1) \sin(\phi_2) + \sin(2\theta_1) \cos(\phi_2) (P_T^2 \cos(2\phi_1) - 1))). \end{aligned} \quad (B2)$$

The other r_M^L unlisted are equal to zero.

B.3. χ_{c2}

The multipole parameters r_M^L for χ_{c2} are expressed as

$$\begin{aligned} r_0^0 &= \frac{1}{64} \{ 4x^2 \cos(2\phi_1) \sin^2(\theta_1) P_T^2 + 54y^2 \cos(2\phi_1) \sin^2(\theta_1) P_T^2 + 108x^2 \cos(4\theta_2) \cos(2\phi_1) \sin^2(\theta_1) P_T^2 \\ &\quad + 18y^2 \cos(4\theta_2) \cos(2\phi_1) \sin^2(\theta_1) P_T^2 - 72 \cos(4\theta_2) \cos(2\phi_1) \sin^2(\theta_1) P_T^2 + 72x^2 \cos(2\phi_1) \cos(2\phi_2) \sin^2(\theta_2) P_T^2 \\ &\quad + 108y^2 \cos(2\phi_1) \cos(2\phi_2) \sin^2(\theta_2) P_T^2 - 144 \cos(2\phi_1) \cos(2\phi_2) \sin^2(\theta_2) P_T^2 \\ &\quad + 48x^2 \cos(2\phi_1) \cos(\phi_2) \sin(2\theta_1) \sin(2\theta_2) P_T^2 - 72y^2 \cos(2\phi_1) \cos(\phi_2) \sin(2\theta_1) \sin(2\theta_2) P_T^2 \\ &\quad + 48 \cos(2\phi_1) \cos(\phi_2) \sin(2\theta_1) \sin(2\theta_2) P_T^2 - 72x^2 \cos(2\phi_1) \cos(\phi_2) \sin(2\theta_1) \sin(4\theta_2) P_T^2 \\ &\quad - 12y^2 \cos(2\phi_1) \cos(\phi_2) \sin(2\theta_1) \sin(4\theta_2) P_T^2 + 48 \cos(2\phi_1) \cos(\phi_2) \sin(2\theta_1) \sin(4\theta_2) P_T^2 \\ &\quad + 96x^2 \sin(\theta_1) \sin(2\theta_2) \sin(2\phi_1) \sin(\phi_2) P_T^2 - 144y^2 \sin(\theta_1) \sin(2\theta_2) \sin(2\phi_1) \sin(\phi_2) P_T^2 \\ &\quad + 96 \sin(\theta_1) \sin(2\theta_2) \sin(2\phi_1) \sin(\phi_2) P_T^2 - 144x^2 \sin(\theta_1) \sin(4\theta_2) \sin(2\phi_1) \sin(\phi_2) P_T^2 \\ &\quad - 24y^2 \sin(\theta_1) \sin(4\theta_2) \sin(2\phi_1) \sin(\phi_2) P_T^2 + 96 \sin(\theta_1) \sin(4\theta_2) \sin(2\phi_1) \sin(\phi_2) P_T^2 \\ &\quad + 48(2x^2 + 3y^2 - 4) \cos(\theta_1) \sin^2(\theta_2) \sin(2\phi_1) \sin(2\phi_2) P_T^2 + 48x^2 \cos(2\phi_2) \sin^2(\theta_1) \sin^2(\theta_2) \\ &\quad + 72y^2 \cos(2\phi_2) \sin^2(\theta_1) \sin^2(\theta_2) - 96 \cos(2\phi_2) \sin^2(\theta_1) \sin^2(\theta_2) + 18x^2 \cos(4\theta_2) + 3y^2 \cos(4\theta_2) \\ &\quad + \cos(2\theta_1) \{ 2x^2 + 27y^2 + 12P_T^2(2x^2 + 3y^2 - 4) \cos(2\phi_1) \cos(2\phi_2) \sin^2(\theta_2) + 9(6x^2 + y^2 - 4) \cos(4\theta_2) \\ &\quad + 12 \cos(2\theta_2) [-2x^2 + 5y^2 + P_T^2(6x^2 + y^2 - 4) \cos(2\phi_1) \cos(2\phi_2) \sin^2(\theta_2) - 4] - 12 \} - 48x^2 \cos(\phi_2) \sin(2\theta_1) \sin(2\theta_2) \\ &\quad + 72y^2 \cos(\phi_2) \sin(2\theta_1) \sin(2\theta_2) + 3[50x^2 + 67y^2 - 8P_T^2 \cos(2\phi_1) \sin^2(\theta_1) - 4 \cos(4\theta_2) - 16 \cos(\phi_2) \sin(2\theta_1) \sin(2\theta_2) + 52] \\ &\quad + 72x^2 \cos(\phi_2) \sin(2\theta_1) \sin(4\theta_2) + 12y^2 \cos(\phi_2) \sin(2\theta_1) \sin(4\theta_2) - 48 \cos(\phi_2) \sin(2\theta_1) \sin(4\theta_2) \\ &\quad + 12 \cos(2\theta_2) [\cos(2\phi_1) (3(6x^2 + y^2 - 4) \cos(2\phi_2) \sin^2(\theta_2) - 2(2x^2 - 5y^2 + 4) \sin^2(\theta_1)) P_T^2 - 6x^2 + 7y^2 \\ &\quad + 2(6x^2 + y^2 - 4) \sin^2(\theta_2) (2 \cos(\theta_1) \sin(2\phi_1) \sin(2\phi_2) P_T^2 + \cos(2\phi_2) \sin^2(\theta_1) - 4)] a_{1,0}^2 b_{1,0}^2, \\ r_0^0 r_{-1}^1 &= \frac{3}{64} a_{1,0}^2 b_{1,0}^2 \{ 2x \sin \Delta_1 \{ \sin(2\theta_2) [4 \sin^2(\theta_1) \cos(2\phi_2) + \cos(2\theta_1) (4P_T^2 \cos(2\phi_1) \cos^2(\phi_2) - 2) \\ &\quad + 2P_T^2 \cos(2\phi_1) (3 \cos(2\phi_2) - 1) - 6] + 18P_T^2 \sin(4\theta_2) \sin^2(\phi_2) \cos(2\phi_1) - 3 \sin(4\theta_2) [2 \sin^2(\theta_1) \cos(2\phi_2) + \cos(2\theta_1) \\ &\quad \times (P_T^2 \cos(2\phi_1) (\cos(2\phi_2) + 3) - 3) - 1] - 8P_T^2 \sin(\theta_1) [\cos(2\theta_2) - 3 \cos(4\theta_2)] \sin(2\phi_1) \sin(\phi_2) \} \\ &\quad + 8 \cos(\theta_1) \{ x \sin \Delta_1 [P_T^2 (2 \sin(2\theta_2) - 3 \sin(4\theta_2)) \sin(2\phi_1) \sin(2\phi_2) \\ &\quad - 2 \sin(\theta_1) (\cos(2\theta_2) - 3 \cos(4\theta_2)) \cos(\phi_2) (P_T^2 \cos(2\phi_1) - 1)] \\ &\quad + \sqrt{6} y \sin(\Delta_1 - \Delta_2) [\sin(\theta_1) (3 \cos(2\theta_2) + \cos(4\theta_2)) \cos(\phi_2) (P_T^2 \cos(2\phi_1) - 1) \\ &\quad - 4P_T^2 \sin(\theta_2) \cos^3(\theta_2) \sin(2\phi_1) \sin(2\phi_2)] \} \\ &\quad + \sqrt{6} y \sin(\Delta_1 - \Delta_2) \{ 6P_T^2 \sin(4\theta_2) \sin^2(\phi_2) \cos(2\phi_1) - 2 \sin(2\theta_2) [2 \sin^2(\theta_1) \cos(2\phi_2) \\ &\quad + \cos(2\theta_1) (P_T^2 \cos(2\phi_1) (\cos(2\phi_2) + 5) - 5) + P_T^2 \cos(2\phi_1) (3 \cos(2\phi_2) - 5) - 7] - \sin(4\theta_2) (2 \sin^2(\theta_1) \cos(2\phi_2) \\ &\quad + \cos(2\theta_1) (P_T^2 \cos(2\phi_1) (\cos(2\phi_2) + 3) - 3) - 1] + 8P_T^2 \sin(\theta_1) (3 \cos(2\theta_2) + \cos(4\theta_2)) \sin(2\phi_1) \sin(\phi_2) \} \}, \end{aligned}$$

$$\begin{aligned}
r_0^0 r_1^1 &= \frac{3}{224} a_{1,0}^2 b_{1,0}^2 \{ 7 \sin(\theta_2) [\sin(2\phi_2) (2 \sin^2(\theta_1) + P_T^2 (\cos(2\theta_1) + 3) \cos(2\phi_1)) \\
&\quad - 4P_T^2 \cos(\theta_1) \sin(2\phi_1) \cos(2\phi_2)] [2x \sin \Delta_1 (3 \cos(2\theta_2) + 1) \\
&\quad + \sqrt{6}y \sin(\Delta_1 - \Delta_2) (\cos(2\theta_2) + 3)] + 28 \sin(\theta_1) \cos(\theta_2) [\cos(\theta_1) \sin(\phi_2) (1 - P_T^2 \cos(2\phi_1)) \\
&\quad + P_T^2 \sin(2\phi_1) \cos(\phi_2)] [2x \sin \Delta_1 (3 \cos(2\theta_2) - 1) + \sqrt{6}y \sin(\Delta_1 - \Delta_2) (\cos(2\theta_2) + 3)] \}, \\
r_0^0 r_{-2}^2 &= -\frac{3xy}{8\sqrt{2}} a_{1,0}^2 b_{1,0}^2 \cos(\Delta_2) \{ -\cos(\theta_2) (3 \cos(2\theta_2) + 1) \sin(2\phi_2) [2 \sin^2(\theta_1) + P_T^2 (\cos(2\theta_1) + 3) \cos(2\phi_1)] \\
&\quad + 2P_T^2 \sin(2\phi_1) [\cos(\theta_1) (5 \cos(\theta_2) + 3 \cos(3\theta_2)) \cos(2\phi_2) + \sin(\theta_1) (7 \sin(\theta_2) + 3 \sin(3\theta_2)) \cos(\phi_2)] \\
&\quad - 2 \sin(2\theta_1) \sin(\theta_2) (3 \cos(2\theta_2) + 5) \sin(\phi_2) (P_T^2 \cos(2\phi_1) - 1) \} \\
r_0^0 r_{-1}^2 &= -\frac{3}{224} a_{1,0}^2 b_{1,0}^2 \{ 2x \cos \Delta_1 \{ 14 \cos(\theta_2) (3 \cos(2\theta_2) - 1) (2P_T^2 \sin(\theta_1) \sin(2\phi_1) \cos(\phi_2) \\
&\quad + \sin(2\theta_1) \sin(\phi_2) (1 - P_T^2 \cos(2\phi_1))) - 7 \sin(\theta_2) (3 \cos(2\theta_2) + 1) [4P_T^2 \cos(\theta_1) \sin(2\phi_1) \cos(2\phi_2) \\
&\quad - \sin(2\phi_2) (2 \sin^2(\theta_1) + P_T^2 (\cos(2\theta_1) + 3) \cos(2\phi_1))] \} \\
&\quad + 7 \sqrt{6}y \cos(\Delta_1 - \Delta_2) \{ \sin(\theta_2) (\cos(2\theta_2) + 3) \sin(2\phi_2) (2 \sin^2(\theta_1) + P_T^2 (\cos(2\theta_1) + 3) \cos(2\phi_1)) \\
&\quad - 2P_T^2 (5 \sin(\theta_2) + \sin(3\theta_2)) \cos(\theta_1) \sin(2\phi_1) \cos(2\phi_2) + \sin(2\theta_1) \cos(3\theta_2) \sin(\phi_2) (1 - P_T^2 \cos(2\phi_1)) \\
&\quad + \cos(\theta_2) (4P_T^2 \sin(\theta_1) (\cos(2\theta_2) + 3) \sin(2\phi_1) \cos(\phi_2) - 7 \sin(2\theta_1) \sin(\phi_2) (P_T^2 \cos(2\phi_1) - 1)) \}, \\
r_0^0 r_0^2 &= \frac{1}{128} \{ 4x^2 \cos(2\phi_1) \sin^2(\theta_1) P_T^2 + 54y^2 \cos(2\phi_1) \sin^2(\theta_1) P_T^2 + 108x^2 \cos(4\theta_2) \cos(2\phi_1) \sin^2(\theta_1) P_T^2 \\
&\quad + 18y^2 \cos(4\theta_2) \cos(2\phi_1) \sin^2(\theta_1) P_T^2 + 144 \cos(4\theta_2) \cos(2\phi_1) \sin^2(\theta_1) P_T^2 + 48 \cos(2\phi_1) \sin^2(\theta_1) P_T^2 \\
&\quad + 72x^2 \cos(2\phi_1) \cos(2\phi_2) \sin^2(\theta_2) P_T^2 + 108y^2 \cos(2\phi_1) \cos(2\phi_2) \sin^2(\theta_2) P_T^2 + 288 \cos(2\phi_1) \cos(2\phi_2) \sin^2(\theta_2) P_T^2 \\
&\quad + 48x^2 \cos(2\phi_1) \cos(\phi_2) \sin(2\theta_1) \sin(2\theta_2) P_T^2 - 72y^2 \cos(2\phi_1) \cos(\phi_2) \sin(2\theta_1) \sin(2\theta_2) P_T^2 \\
&\quad - 96 \cos(2\phi_1) \cos(\phi_2) \sin(2\theta_1) \sin(2\theta_2) P_T^2 - 72x^2 \cos(2\phi_1) \cos(\phi_2) \sin(2\theta_1) \sin(4\theta_2) P_T^2 \\
&\quad - 12y^2 \cos(2\phi_1) \cos(\phi_2) \sin(2\theta_1) \sin(4\theta_2) P_T^2 - 96 \cos(2\phi_1) \cos(\phi_2) \sin(2\theta_1) \sin(4\theta_2) P_T^2 \\
&\quad + 96x^2 \sin(\theta_1) \sin(2\theta_2) \sin(2\phi_1) \sin(\phi_2) P_T^2 - 144y^2 \sin(\theta_1) \sin(2\theta_2) \sin(2\phi_1) \sin(\phi_2) P_T^2 \\
&\quad - 192 \sin(\theta_1) \sin(2\theta_2) \sin(2\phi_1) \sin(\phi_2) P_T^2 - 144x^2 \sin(\theta_1) \sin(4\theta_2) \sin(2\phi_1) \sin(\phi_2) P_T^2 \\
&\quad - 24y^2 \sin(\theta_1) \sin(4\theta_2) \sin(2\phi_1) \sin(\phi_2) P_T^2 - 192 \sin(\theta_1) \sin(4\theta_2) \sin(2\phi_1) \sin(\phi_2) P_T^2 \\
&\quad + 48(2x^2 + 3y^2 + 8) \cos(\theta_1) \sin^2(\theta_2) \sin(2\phi_1) \sin(2\phi_2) P_T^2 + 150x^2 + 201y^2 + 48x^2 \cos(2\phi_2) \sin^2(\theta_1) \sin^2(\theta_2) \\
&\quad + 72y^2 \cos(2\phi_2) \sin^2(\theta_1) \sin^2(\theta_2) + 192 \cos(2\phi_2) \sin^2(\theta_1) \sin^2(\theta_2) + 18x^2 \cos(4\theta_2) + 3y^2 \cos(4\theta_2) + 24 \cos(4\theta_2) \\
&\quad + \cos(2\theta_1) [2x^2 + 27y^2 + 12P_T^2 (2x^2 + 3y^2 + 8) \cos(2\phi_1) \cos(2\phi_2) \sin^2(\theta_2) + 9(6x^2 + y^2 + 8) \cos(4\theta_2) \\
&\quad + 12 \cos(2\theta_2) [-2x^2 + 5y^2 + P_T^2 (6x^2 + y^2 + 8) \cos(2\phi_1) \cos(2\phi_2) \sin^2(\theta_2) + 8] + 24] - 48x^2 \cos(\phi_2) \sin(2\theta_1) \sin(2\theta_2) \\
&\quad + 72y^2 \cos(\phi_2) \sin(2\theta_1) \sin(2\theta_2) + 96 \cos(\phi_2) \sin(2\theta_1) \sin(2\theta_2) + 72x^2 \cos(\phi_2) \sin(2\theta_1) \sin(4\theta_2) \\
&\quad + 12y^2 \cos(\phi_2) \sin(2\theta_1) \sin(4\theta_2) + 96 \cos(\phi_2) \sin(2\theta_1) \sin(4\theta_2) + 12 \cos(2\theta_2) \{\cos(2\phi_1) [2(-2x^2 + 5y^2 + 8) \sin^2(\theta_1) \\
&\quad + 3(6x^2 + y^2 + 8) \cos(2\phi_2) \sin^2(\theta_2)] P_T^2 - 6x^2 + 7y^2 + 2(6x^2 + y^2 + 8) \sin^2(\theta_2) (2 \cos(\theta_1) \sin(2\phi_1) \sin(2\phi_2) P_T^2 \\
&\quad + \cos(2\phi_2) \sin^2(\theta_1)) + 8\} - 312\} a_{1,0}^2 b_{1,0}^2, \\
r_0^0 r_1^2 &= \frac{3}{224} \{ 7 \sqrt{\frac{3}{2}} y \cos(\Delta_1 - \Delta_2) \{ -32P_T^2 \cos(\theta_1) \sin(\theta_2) \sin(2\phi_1) \sin(2\phi_2) \cos^3(\theta_2) \\
&\quad + 20P_T^2 \cos(2\phi_1) \sin^2(\theta_1) \sin(2\theta_2) - 4 \cos(2\phi_2) \sin^2(\theta_1) \sin(2\theta_2) + 2[5 \cos(2\theta_1) + \cos(2\theta_2) + 7] \sin(2\theta_2) \\
&\quad - 6P_T^2 \cos(2\phi_1) \cos(2\phi_2) \sin(2\theta_2) - 2P_T^2 \cos(2\theta_1) \cos(2\phi_1) \cos(2\phi_2) \sin(2\theta_2) + 6P_T^2 \cos(2\phi_1) \sin^2(\theta_1) \sin(4\theta_2)
\}
\end{aligned}$$

$$\begin{aligned}
& -2 \cos(2\phi_2) \sin^2(\theta_1) \sin(4\theta_2) + 3 \cos(2\theta_1) \sin(4\theta_2) - 3 P_T^2 \cos(2\phi_1) \cos(2\phi_2) \sin(4\theta_2) \\
& - P_T^2 \cos(2\theta_1) \cos(2\phi_1) \cos(2\phi_2) \sin(4\theta_2) + 12 \cos(2\theta_2) (2 \sin(\theta_1) \sin(2\phi_1) \sin(\phi_2) P_T^2 \\
& + (P_T^2 \cos(2\phi_1) - 1) \cos(\phi_2) \sin(2\theta_1)) + 4 \cos(4\theta_2) (2 \sin(\theta_1) \sin(2\phi_1) \sin(\phi_2) P_T^2 \\
& + (P_T^2 \cos(2\phi_1) - 1) \cos(\phi_2) \sin(2\theta_1)) - 7x \cos \Delta_1 \{4 \cos(2\phi_1) \sin^2(\theta_1) \sin(2\theta_2) P_T^2 \\
& - 2 \cos(2\theta_1) \cos(2\phi_1) \cos(2\phi_2) \sin(2\theta_2) P_T^2 - 6 \cos(2\phi_1) \cos(2\phi_2) \sin(2\theta_2) P_T^2 - 18 \cos(2\phi_1) \sin^2(\theta_1) \sin(4\theta_2) P_T^2 \\
& + 3 \cos(2\theta_1) \cos(2\phi_1) \cos(2\phi_2) \sin(4\theta_2) P_T^2 + 9 \cos(2\phi_1) \cos(2\phi_2) \sin(4\theta_2) P_T^2 + 4 \cos(\theta_1) (3 \sin(4\theta_2) \\
& - 2 \sin(2\theta_2)) \sin(2\phi_1) \sin(2\phi_2) P_T^2 - 4 \cos(2\phi_2) \sin^2(\theta_1) \sin(2\theta_2) + 2 (\cos(2\theta_1) + 3) \sin(2\theta_2) \\
& + 6 \cos(2\phi_2) \sin^2(\theta_1) \sin(4\theta_2) - 9 \cos(2\theta_1) \sin(4\theta_2) - 3 \sin(4\theta_2) + 4 \cos(2\theta_2) [2 \sin(\theta_1) \sin(2\phi_1) \sin(\phi_2) P_T^2 \\
& + (P_T^2 \cos(2\phi_1) - 1) \cos(\phi_2) \sin(2\theta_1)] + 12 \cos(4\theta_2) [(1 - P_T^2 \cos(2\phi_1)) \cos(\phi_2) \sin(2\theta_1) \\
& - 2 P_T^2 \sin(\theta_1) \sin(2\phi_1) \sin(\phi_2)]\} a_{1,0}^2 b_{1,0}^2, \\
r_0^0 r_2^2 &= \frac{3xy}{32\sqrt{2}} a_{1,0}^2 b_{1,0}^2 \cos(\Delta_2) \{2 \sin^2(\theta_1) (4 \cos(2\theta_2) + 3 \cos(4\theta_2) + 9) \cos(2\phi_2) + 4 \sin^2(\theta_2) (3 (\cos(2\theta_2) + 3) \\
& + \cos(2\theta_1) (9 \cos(2\theta_2) + 11)) + P_T^2 \cos(2\phi_1) [(\cos(2\theta_1) + 3) (4 \cos(2\theta_2) + 3 \cos(4\theta_2) + 9) \cos(2\phi_2) \\
& + 4 \sin(2\theta_1) (2 \sin(2\theta_2) + 3 \sin(4\theta_2)) \cos(\phi_2) + 8 \sin^2(\theta_1) \sin^2(\theta_2) (9 \cos(2\theta_2) + 11)] + 4 P_T^2 \cos(\theta_1) (4 \cos(2\theta_2) \\
& + 3 \cos(4\theta_2) + 9) \sin(2\phi_1) \sin(2\phi_2) - 4 (2 \sin(2\theta_2) + 3 \sin(4\theta_2)) (\sin(2\theta_1) \cos(\phi_2) - 2 P_T^2 \sin(\theta_1) \sin(2\phi_1) \sin(\phi_2))\}.
\end{aligned} \tag{B3}$$

C. Monte Carlo Simulation and Fit Results of the angular distributions

Table 5. Monte Carlo simulation and fit results of the projection of the polar angles in the processes $\psi(2S) \rightarrow \gamma\chi_{c0}$, and $\psi(2S) \rightarrow \gamma\chi_{c1,2}$

Decay mode	Default α value	Fitted α value	Figure
$\psi(2S) \rightarrow \gamma\chi_{c0}$	1.00	1.00 ± 0.01	8(a)
$\omega \rightarrow \pi^+ \pi^- \pi^0$	-1.00	-1.00 ± 0.01	8(b)
$\psi(2S) \rightarrow \gamma\chi_{c0}$	1.00	1.02 ± 0.01	9(a)
$\rho^0 \rightarrow \pi^+ \pi^-$	-1.00	-1.00 ± 0.01	9(b)
$\psi(2S) \rightarrow \gamma\chi_{c1}$ ($\chi_{c1} \rightarrow \gamma\rho$)	-0.33	-0.34 ± 0.01	10(a)
$\psi(2S) \rightarrow \gamma\chi_{c1}$ ($\chi_{c1} \rightarrow \gamma\omega$)	-0.33	-0.33 ± 0.01	11(a)
$\psi(2S) \rightarrow \gamma\chi_{c2}$ ($\chi_{c2} \rightarrow \gamma\rho$)	0.08	0.07 ± 0.01	12(a)
$\psi(2S) \rightarrow \gamma\chi_{c2}$ ($\chi_{c2} \rightarrow \gamma\omega$)	0.08	0.07 ± 0.01	13(a)

Table 6. Monte Carlo simulation and fit results in the decays $\chi_{c1,2} \rightarrow \gamma V$

Decay mode	Input value	Fit value	Figure
$\chi_{c0} \rightarrow \gamma\rho$	$P_T = 0.24$	$P_T = 0.24 \pm 0.01$	9(c)
$\chi_{c0} \rightarrow \gamma\omega$	$P_T = 0.24$	$P_T = 0.25 \pm 0.01$	8(c)
$\chi_{c1} \rightarrow \gamma\rho$	$x = 0.43, P_T = 0.24$	$x = 0.43 \pm 0.01, P_T = 0.25 \pm 0.02$	10(b), 10(c), 10(d)
$\chi_{c1} \rightarrow \gamma\omega$	$x = 0.57, P_T = 0.24$	$x = 0.56 \pm 0.01, P_T = 0.23 \pm 0.02$	11(b), 11(c), 11(d)
$\chi_{c2} \rightarrow \gamma\rho$	$x = 1.55, y = 2.06, P_T = 0.24$	$x = 1.58 \pm 0.79, y = 2.09 \pm 0.77, P_T = 0.29 \pm 0.07$	12(b), 12(c), 12(d)
$\chi_{c2} \rightarrow \gamma\omega$	$x = 0, y = 1, P_T = 0.24$	$x = 0.00 \pm 0.02, y = 1.00 \pm 0.02, P_T = 0.22 \pm 0.01$	13(b), 13(c), 13(d)

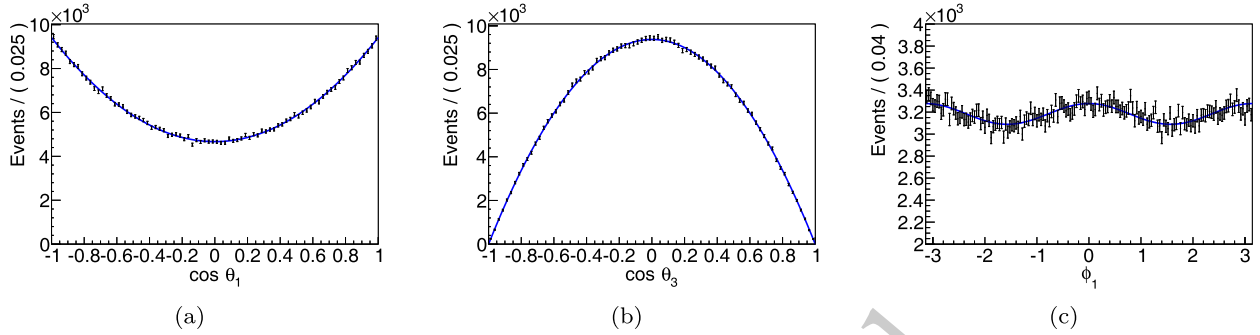


Fig. 9. (color online) $dN/d\cos\theta_1$, $dN/d\cos\theta_3$ and $dN/d\phi_1$ distributions versus $\cos\theta_1$, $\cos\theta_3$ and ϕ_1 in $\psi(2S) \rightarrow \gamma\chi_{c0}$ and $\rho^0 \rightarrow \pi^+\pi^-$ from $\chi_{c0} \rightarrow \gamma\rho$ decays. Dots with error bars are filled with MC events, and the blue solid curve denotes the fit.

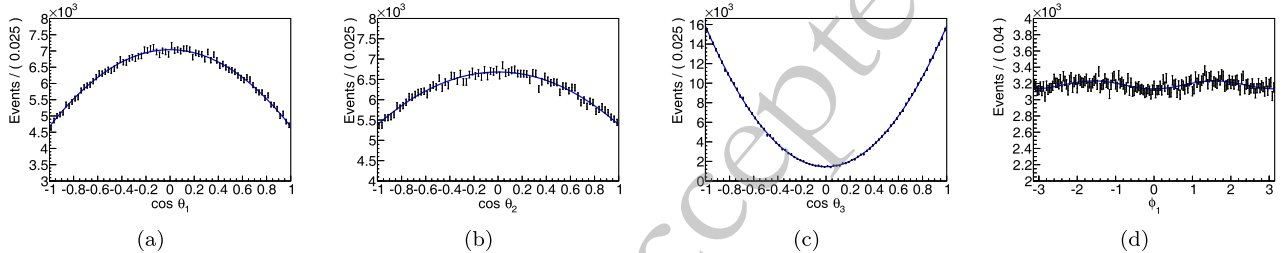


Fig. 10. (color online) $dN/d\cos\theta_i, i = 1, 2, 3$ and $dN/d\phi_1$ distributions versus $\cos\theta_i$ and ϕ_1 in $\psi(2S) \rightarrow \gamma\chi_{c1}$, $\chi_{c1} \rightarrow \gamma\rho$ and $\rho^0 \rightarrow \pi^+\pi^-$ decays. Dots with error bars are filled with MC events, and the blue solid curve denotes the fit.

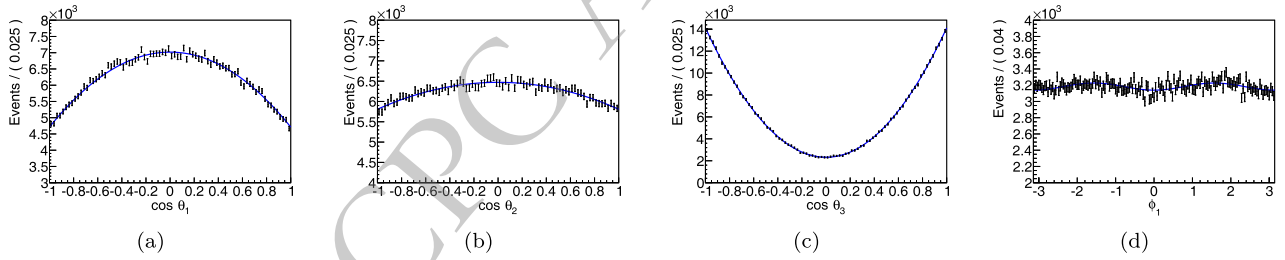


Fig. 11. (color online) $dN/d\cos\theta_i, i = 1, 2, 3$ and $dN/d\phi_1$ distributions versus $\cos\theta_i$ and ϕ_1 in $\psi(2S) \rightarrow \gamma\chi_{c1}$, $\chi_{c1} \rightarrow \gamma\omega$ and $\omega \rightarrow \pi^+\pi^-\pi^0$ decays. Dots with error bars are filled with MC events, and the blue solid curve denotes the fit.

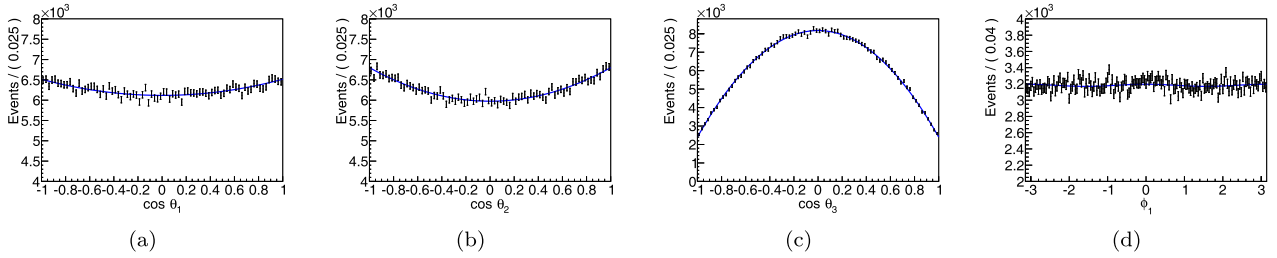


Fig. 12. (color online) Fits to the angular distributions of $\cos\theta_i (i = 1, 2, 3)$ and $dN/d\phi_1$ versus $\cos\theta_i$ and ϕ_1 in $\psi(2S) \rightarrow \gamma\chi_{c2}$, $\chi_{c2} \rightarrow \gamma\rho$ and $\rho^0 \rightarrow \pi^+\pi^-$ decays. Dots with error bars represent MC events, and the blue solid curve denotes the fit.

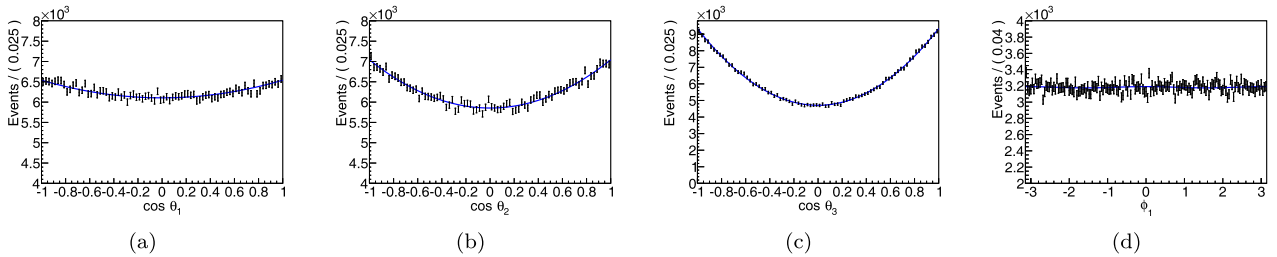


Fig. 13. (color online) $dN/d\cos\theta_i, i = 1, 2, 3$ and $dN/d\phi_1$ distributions versus $\cos\theta_i$ and ϕ_1 in $\psi(2S) \rightarrow \gamma\chi_{c2}$, $\chi_{c2} \rightarrow \gamma\omega$ and $\omega \rightarrow \pi^+\pi^-\pi^0$ decays. Dots with error bars are filled with MC events, and the blue solid curve denotes the fit.

References

- [1] R. L. Workman *et al.* [Particle Data Group], PTEP **2022**, 083C01 (2022)
- [2] T. Barnes, S. Godfrey and E. S. Swanson, Phys. Rev. D **72**, 054026 (2005)
- [3] N. Brambilla, S. Eidelman, B. K. Heltsley, R. Vogt, G. T. Bodwin, E. Eichten, A. D. Frawley, A. B. Meyer, R. E. Mitchell and V. Papadimitriou, *et al.*, Eur. Phys. J. C **71**, 1534 (2011)
- [4] Y. J. Gao, Y. J. Zhang and K. T. Chao, Chin. Phys. Lett. **23**, 2376 (2006)
- [5] Y. J. Gao, Y. J. Zhang and K. T. Chao, [arXiv: hep-ph/0701009 [hep-ph]].
- [6] J. V. Bennett *et al.* [CLEO Collaboration], Phys. Rev. Lett. **101**, 151801 (2008)
- [7] M. Ablikim *et al.* [BESIII Collaboration], Phys. Rev. D **83**, 112005 (2011)
- [8] D. Y. Chen, Y. B. Dong and X. Liu, Eur. Phys. J. C **70**, 177 (2010)
- [9] A. A. Sokolov and I. M. Ternov, Dokl. Akad. Nauk SSSR **153**, 1052 (1963)
- [10] M. Ablikim *et al.* [BESIII Collaboration], [arXiv: 2403.06766 [hep-ex]].
- [11] S. U. Chung, Phys. Rev. D **48**, 1225 (1993) [erratum: Phys. Rev. D **56**, 4419 (1997)].
- [12] S. U. Chung, Phys. Rev. D **57**, 431 (1998)
- [13] S. U. Chung, CERN, Geneva, 1969-1970, CERN Yellow Reports: Monographs doi: 10.5170/CERN-1971-008.
- [14] P. C. Hong, F. Yan, R. G. Ping and T. Luo, Chin. Phys. C **47**, 053101 (2023)
- [15] G. Karl, S. Meshkov and J. L. Rosner, Phys. Rev. D **13**, 1203 (1976)
- [16] N. Kivel and M. Vanderhaeghen, Phys. Rev. D **96**, 054007 (2017)
- [17] M. G. Doncel, P. Mery, L. Michel, P. Minnaert and K. C. Wali, Phys. Rev. D **7**, 815 (1973)
- [18] H. Chen and R. G. Ping, Phys. Rev. D **102**, 016021 (2020)
- [19] X. Cao, Y. T. Liang and R. G. Ping, Phys. Rev. D **110**, 014035 (2024)
- [20] M. Ablikim *et al.* [BESIII Collaboration], Phys. Rev. D **84**, 092006 (2011)
- [21] M. Ablikim *et al.* [BESIII Collaboration], Chin. Phys. C **44**, 040001 (2020)
- [22] M. Achasov, X. C. Ai, R. Aliberti, L. P. An, Q. An, X. Z. Bai, Y. Bai, O. Bakina, A. Barnyakov and V. Blinov, *et al.*, Front. Phys. (Beijing) **19**, 14701 (2024)
- [23] T. Z. Han, R. G. Ping, T. Luo and G. Z. Xu, Chin. Phys. C **44**, 013002 (2020)
- [24] T. Aushev, W. Bartel, A. Bondar, J. Brodzicka, T. E. Browder, P. Chang, Y. Chao, K. F. Chen, J. Dalseno and A. Drutskoy, *et al.* [arXiv: 1002.5012 [hep-ex]].